



**NOVA**  
NOVA SCHOOL OF  
SCIENCE & TECHNOLOGY

DEPARTMENT OF  
CHEMISTRY

ANA LUÍSA DA SILVA RIBEIRO BENAVENTE  
BSc in Biochemistry

Development of an *in vitro* model of mucinous  
tumors

MASTER IN BIOTECHNOLOGY  
NOVA University Lisbon  
October, 2022





## Development of an *in vitro* model of mucinous tumors

**Ana Luísa da Silva Ribeiro Benavente**

BSc in Biochemistry

**Adviser:** Thomas Crouzier  
*Doctor, KTH Royal Institute of Technology*

**Co-adviser:** Filomena Freitas  
*Doctor, NOVA School of Science and Technology*

### **Examination Committee:**

**Rapporteur:** Sofia Costa-Lima,  
*Doctor, ICBAS University of Porto*

**Adviser:** Thomas Crouzier,  
*Doctor, Royal Institute of Technology*



## **Development of an *in vitro* model of mucinous tumors**

Copyright © <Ana Luísa Benavente>, NOVA School of Science and Technology, NOVA University Lisbon.

The NOVA School of Science and Technology and the NOVA University Lisbon have the right, perpetual and without geographical boundaries, to file and publish this dissertation through printed copies reproduced on paper or on digital form, or by any other means known or that may be invented, and to disseminate through scientific repositories and admit its copying and distribution for non-commercial, educational or research purposes, as long as credit is given to the author and editor.

This document was created with Microsoft Word text processor and the NOVAthesis Word template [1].



Dedicatory lorem ipsum.





## ACKNOWLEDGMENTS

I would like to genuinely thank my main supervisor Dr. Thomas Crouzier, who always provided me with a perfect equilibrium between guidance and autonomy. I deeply appreciate the shared enthusiasm over every small step taken throughout this project, as well as all the interesting brainstorming meetings to decide on different approaches. Merci!

Countless thanks to every member of the Crouzier group and the Division of Glycoscience as a whole. At some point in the last year, all of you took time to help me in one way or another. Thank you, Dr. Sedef Ilk for your kindness and serenity within the working environment and for your continuous promptitude to help me. A special thanks to Dr. Kun Jiang for his endless patience and availability to give me innumerable valuable insights during experiments. Thank you to NOVA School of Science and Technology and Royal Institute of Technology for smoothly cooperating with the Erasmus + initiative. To my co-supervisor Dr. Filomena Freitas, I appreciate your willingness to help me and follow up on the progress made.

To my closest friends and boyfriend Sergio, I am deeply sorry that you couldn't be in the presence of my hilarious and charming self as frequently. But seriously, thank you for just being who you are and caring for me. Inês and Miguel, after so many Zoom classes look at us! Couldn't have asked for a better duo to share this adventure with. Catarina, my best friend for life, even if you were also overwhelmed with your master's thesis in Munich, you always made time to catch up and visit me.

To all the wonderful friends I made at KTH, you made my days incomparably happier. Alma, Kasra and Valentina, every moment spent with you was on the verge of chaos- a good type of chaos that I'll miss a lot. Kasane, I profoundly appreciate every conversation, memory and fika along the way. Some extra thanks for teaching me origami. Abby and Beatriz, you are the definition of double trouble. Thanks gals for making everything sound like a fantastic plan, even if it includes sitting out in the cold hoping to see the northern lights or embarking on a random ship to Tallin. Julia, Lova and Vicky, you were there until the very end. Even in gloomy days our sarcasm and irony never failed to make us smile. I'll forever cherish our memories together.

Words can not express how grateful I am for my family and Sergio's family. Specially, thank you mom and dad for allowing me to live this experience. Finally, thanks to my big brother Stefano for always keeping me grounded (and doubting I would survive the Swedish winter).



“For the things we have to learn before we can do them, we learn by doing them”  
(Aristotle).



## ABSTRACT

Mucinous carcinomas are tumors with poor prognosis and secrete a large amount of mucus. The development of an *in vitro* model that reconstitutes the mucin-rich microenvironment of mucinous carcinomas can provide a better understanding on how the aberrant mucus production relates to the progression of these tumors. Furthermore, it responds to the lack of predictive *in vitro* models and leads the way to the replacement of standard animal models.

In this project, colorectal mucinous carcinomas are studied, for which several mucin-secreting cell lines are available. We demonstrate that crosslinked bovine submaxillary mucin gels function as a platform to encapsulate cancer cells and obtain spheroids that grow and proliferate over 10 days. More importantly, they resist 5-FU and the drug resistance was different between cell lines. Although at a slower rate than HT-29 MTX, LS174T cells reached equivalent spheroids diameter (156.5 and 187.9  $\mu\text{m}$ , respectively) and metabolic activity (3- and 4- fold increases, respectively). LS174T also showed the greater physical barrier effect against 5-FU in monolayer (2D) or encapsulated (3D) in BSM, but also a potential biological barrier caused by cell entanglement in mucin-gel for 10 days. In the 2D model, LS174T cell viability went from  $45.9 \pm 8.81\%$  without gel to  $84.2 \pm 1.96\%$  with muc-gel covering the cells. When encapsulated and further challenged with 50.0 mM of 5-FU,  $59.6 \pm 7.56\%$  cells were viable after 6 h, whereas  $76.2 \pm 5.20\%$  of cells survived after 10 days of interaction with BSM.

Thus, these results unlock an exciting path to apply mucins as a scaffold for mucinous cancer cells and enlighten necessary refinements to be implemented in future studies towards the ultimate goal of building a robust 3D model capable of recreating the *in vivo* tumor microenvironment and serving as a high-throughput platform for drug screening in the pharmaceutical industry.

**Keywords:** Colorectal cancer, Drug-resistance, Encapsulation, Hydrogel, Mucins, Tumor Micro-environment



## RESUMO

Os carcinomas mucinosos são tumores com uma reduzida oportunidade de recuperação e secretam uma grande quantidade de muco. O desenvolvimento de um modelo *in vitro* que reconstitua o microambiente rico em mucinas de um cancro mucinoso pode proporcionar conhecimentos pertinentes acerca da relação entre a produção irregular de muco e a progressão deste tipo de tumores. Além disso, preenche a lacuna de modelos *in vitro* disponíveis e abre horizontes para a substituição de modelos *standard* de animais.

Este projeto focou-se no cancro colorectal mucinoso, para o qual existem várias linhas celulares secretoras de muco. Demonstra-se que o hidrogel de mucinas funciona para a encapsulação de células de cancro e obtenção de esferóides que crescem e proliferam durante 10 dias. Principalmente, demonstra-se resistência a 5-FU, que diferiu entre linhas celulares. Embora mais lentamente do que as células HT-29 MTX, os esferóides de LS174T atingiram diâmetro e atividade metabólica semelhantes. LS174T revelou um maior efeito de barreira física contra o fármaco 5-FU nos modelos 2D e 3D. Neste último, os resultados sugeriram um potencial efeito biológico resultante da interação das células com BSM durante 10 dias. Constatou-se, no modelo 2D, uma maior viabilidade celular de LS174T na presença de BSM ( $84.2 \pm 1.96\%$ ) comparando com a ausência de hidrogel ( $45.9 \pm 8.81\%$ ). Relativamente à encapsulação e ensaio com 50.0 mM de 5-FU,  $59.6 \pm 7.56\%$  das células eram viáveis após 6 h, enquanto após 10 dias de interação com BSM verificou-se  $76.2 \pm 5.20\%$  de viabilidade.

Estes resultados inauguram um percurso entusiasmante para a aplicação de mucinas como uma plataforma para células de cancros mucinosos e elucidam acerca de melhorias necessárias em estudos futuros, com um objetivo maior: o desenvolvimento de um modelo 3D robusto, capaz de recrear o microambiente *in vivo* tumoral e de ser uma plataforma de alto rendimento para *drug screening* na indústria farmacêutica.

**Palavras chave:** Cancro colorectal, Resistência a medicamentos, Encapsulação, Hidrogel, Mucinas, Microambiente tumoral





# CONTENTS

<b>1</b>	<b>INTRODUCTION.....</b>	<b>26</b>
1.1	Mucins as the major protein component of mucus.....	26
1.1.1	Properties of mucins .....	29
1.1.2	Sources of secreted mucins and muc-gel .....	32
1.2	Mucin-related diseases .....	34
1.2.1	Poor prognosis of CRC and aberrant mucin expression.....	35
1.2.2	Chemotherapy effectiveness against mucinous tumors .....	35
1.2.3	Biomedical applications of mucins.....	36
<b>2</b>	<b>MATERIALS AND METHODS.....</b>	<b>41</b>
2.1	Mucin and alginate gels .....	41
2.1.1	Synthesis of hydrogels .....	41
2.1.2	Rheological properties of BSM.....	42
2.2	Human colorectal adenocarcinoma cells .....	42
2.2.1	Cell culture.....	42
2.2.2	Cell encapsulation in hydrogels .....	43
2.2.3	Cell viability assay .....	43
2.2.4	Drug resistance assay .....	43
2.3	Immunofluorescence .....	45
2.3.1	Staining cells for MDR-1.....	45
2.3.2	Staining cells for CD44 .....	45
2.3.3	Spheroid size evaluation .....	46
2.3.4	Statistical Analysis.....	46

<b>3</b>	<b>RESULTS AND DISCUSSION .....</b>	<b>47</b>
3.1	Click-chemistry of BSM with tetrazine and norbornene forms mucin hydrogels .....	47
3.2	BSM and alginate support the encapsulation of CRC cells .....	48
3.2.1	CRC cells grow in BSM and alginate .....	48
3.2.2	CRC cells are metabolically active in BSM and alginate .....	52
3.3	5-FU efficacy is affected by the presence of BSM and alginate .....	54
3.3.1	BSM acts as a physical barrier against 5-FU.....	54
3.3.2	BSM provides a stronger physical barrier than alginate .....	56
3.4	Encapsulation of CRC cells in BSM hints at a potential biological barrier.....	57
3.5	MDR and CSCs might be behind the drug resistance of CRC cells in BSM.....	60
<b>4</b>	<b>CONCLUSION.....</b>	<b>64</b>
	<b>FUTURE WORK .....</b>	<b>65</b>
<b>5</b>	<b>APPENDIX.....</b>	<b>1</b>
5.1	HT-29 MTX spheroids in BSM and alginate .....	1
5.2	Effect of 5-FU in CRC cells .....	4
5.3	Challenge of 2D model with 5-FU .....	5
5.4	Staining CRC cells previously exposed to Muc- or Alg- gels with MDR-1.....	6
5.5	Staining CRC cells previously exposed to muc- or alg-gel with CD44.....	7

## LIST OF FIGURES

Figure 1.1 A representation of the colon epithelium with a mucus layer surrounding goblet cells- the main mucus producers in the human body. Specification of key constituents of goblet cells that participate in the production of mucus. While membrane mucins are cleaved into two subunits in the endoplasmic reticulum, inserted into the membrane and *N*-glycosylated, secreted mucins are *N*-glycosylated in the endoplasmic reticulum and dimerize via their C-terminal domains. Both types of mucins *O*-glycosylated in the Golgi. Subsequently, the dimers of the secreted mucins undergo N-terminal oligomerization and are loaded into secretory granules. Other non-mucin molecules might form non-covalent interactions with mucins [24].

..... 27

Figure 1.2 An overview of human mucosal surfaces, where mucus protects the epithelial cells through its barrier, hydrating/lubricating and bioactivity effects. The eyes take advantage of a microbial defense system characteristic of mucosal surfaces, and tears contribute with their antimicrobial components (a) [2], [119]. The salivary glands protect against the endless exposure to pathogens in the mouth by secreting antibodies that bind to the mucus layer of the epithelia in the oral cavity (b) [120]. In the respiratory tract, the mucus layer confines potentially dangerous external agents (e.g. pathogens, other particles) and contains cytokines that affect mucus secretion and immune cell activities in case of a respiratory infection (c) [121]. The gastrointestinal mucus layer not only acts as a physical barrier from external agents, but also provides lubrication/hydration in the lumen against adverse environments (e.g. gastric acid and digestive enzymes in the stomach) (d),(e) [122], [123]. Cervical mucus has a barrier effect against infections and also functions as a lubricant during sexual intercourse (f) [124].

..... 28

Figure 1.3 Illustration of gel forming mucin's structure. The extended protein core accommodates two regions: a central hydrophilic region with PTS tandem repeats, thus heavily *O*-glycosylated and the hydrophobic terminal regions that are sparsely *N*-glycosylated. As a result, the high-density glycosylation areas that cause mucins to have a negative charge provide a "bottle brush" arrangement of the oligosaccharides. This is due to the resulting steric hindrance of large molecules and charge repulsion between the glycoconjugates which simultaneously increase the stiffness of the molecule. Meanwhile, the less glycosylated areas

that can either be in between PTS repeats or in the –N and –C terminals, display cysteine-rich regions and other disulfide-rich domains, namely vWF-D, vWF-C and cysteine knots. Therefore, mucins monomers assemble into dimers and then oligomers, which interact with each other via intermolecular bonds and entangle into a hydrogel previously referred to as mucus gel [4], [125], [126]. ..... 29

Figure 1.4 Representation of a mucin monomer to exemplify mucin’s bioactivity. On a larger scale, the mucus gel forms a physical barrier and prompts a multitude of biological responses from bacteria and mammalian cells, deconstructing the primordial idea that mucus consisted of a nonspecific static barrier. Both domains of the protein backbone and the terminal sugars of mucin glycans can operate as ligands. Distinctively, sialic acid residues are capable of shielding antigens from antibody recognition. Another type of interaction involves capturing bioactive molecules into the hydrogel mesh structure. Apart from immune cells, mucins influence bacterial behavior through biofilm formation, swimming and expression of virulence factors [22], [127]. ..... 32

Figure 1.5 Representation of mucin modification following the EDC/NHS coupling and grafting of amine derivatives –Tz and –Nb on the mucin’s protein backbone. Subsequent crosslink into a stable hydrogel when mixed due to the “click chemistry”. The biorthogonal click reaction is specific and irreversible..... 33

Figure 1.6 Scheme of methods to break down the mucin structure, weakening its barrier effect. As earlier mentioned, the non-glycosylated domains are an easy target to proteolytic enzymes, which can cleave peptide bonds. Once proteins are damaged- the mucin protein backbone or any other proteins in the gel- the permeability of the mucus gel is raised (a) [80]. An alternative to deal with mucus overproduction is to resort to chemical agents, namely mucolytics, expectorants and mucokinetics that affect mucin polymerization [128]. N-acetylcysteine (NAC) is an example of a mucolytic with an effect on the mucins crosslinking. It reduces the disulphide bonds responsible for connecting mucin monomers into dimers, multimers etc, hence decreasing mucus viscosity and enlarging the pore size of the mesh [129]. Then, the diffusion of particles is facilitated, which is crucial in diseases characterized by a critical airway obstruction, as cystic fibrosis (b) [130], [131]. Lastly, calcium chelators can be added in order to alter mucin crosslinking. Calcium is vital in providing cationic shielding to maintain negatively charged mucins condensed and securely packed within goblet cell mucus granules. Thus, the process of chelating  $Ca^{2+}$  from mucus is responsible for a fast swelling of the gel and consequently, a more disperse, fluid and hydrated network of mucins (c) [82], [132]. ..... 38

Figure 2.1 Schematic representation of the synthesis of BSM gelling components. .... 41

Figure 2.2 Schematic representation of the 2D model based on the seeding of cancer cells in the bottom layer of each well and a top layer of BSM or alginate covering the cell layer for 24 h. Subsequent administration of 5-FU to the cells and evaluation of cell viability. .... 44

Figure 2.3 Schematic representation of the 3D model, consisting of cancer cells encapsulation in BSM or alginate for 6 h or 10 days. Subsequent administration of 5-FU to the cells and evaluation of cell viability. .... 44

Figure 2.4 Illustration of the staining protocol conducted for the immunofluorescence assay in 8-well glass slides. The cells were seeded in a bottom layer, covered by a top layer of gel (BSM or alginate) similarly to the 2D model previously presented. After 6 h or 10 days, the top layer was removed to allow the staining of cells with antibodies, which otherwise would not penetrate muc- and alg- gels. .... 45

Figure 3.1 Rheological characterization of 2.5% muc-gels. Frequency-dependent viscoelastic behavior of muc-gels was evaluated by a rheometer. The error bars designate the standard deviation as obtained from measurements of  $n = 3$  independent experiments. .... 47

Figure 3.2 Visual representation of the 3D model consisting of CRC cells embedded in hydrogel (BSM or alginate) in 96-well plates. .... 48

Figure 3.3 Images taken under a bright field microscope to observe the diameter of HT-29 MTX spheroids encapsulated in BSM (A) and alginate (B) hydrogels for 10 days. Scale bars: 100, 200, 300 and 500  $\mu\text{m}$ , respectively. .... 49

Figure 3.4 The diameter of HT-29 (A), HT-29 MTX (B) and LS174T (C) cancer spheroids encapsulated in BSM and alginate for 10 days was measured using the Cell Profiler software. Statistical significance was obtained by one-way ANOVA test by Prism 9.0. \*, \*\*, \*\*\*, and \*\*\*\* indicate  $p$  values of  $<0.0332$ , 0.0021, 0.0002, and 0.0001, respectively. The diameter quantification was done based on 18 images captured from  $n = 3$  independent repeats. .... 51

Figure 3.5 The metabolic activity of HT-29, HT-29 MTX and LS174T cells in BSM (A) and alginate (B) assessed by the alamar blue assay. For every condition, the data is normalized to the metabolic activity measurements of day 1. The statistical designation above each time point is a comparison to the previous time point of the same data set. The error bars designate the standard deviation as obtained from measurements of  $n = 3$  independent experiments. Statistical significance was obtained by one-way ANOVA test by Prism 9.0. \*, \*\*, \*\*\*, and \*\*\*\* indicate  $p$  values of  $<0.0332$ , 0.0021, 0.0002, and 0.0001, respectively. .... 52

Figure 3.6 Visual representation of the 2D model used in the drug resistance assay. In each well of a 96-well plate there were two layers: a bottom layer with seeded CRC cells and a top layer of hydrogel covering the cells. 5-FU was added at different concentrations for 24 h and a cell metabolic activity assay was carried out. .... 54

Figure 3.7 Cell metabolic activity of HT-29, HT-29 MTX and LS174T either without hydrogel on the top layer or with BSM and a subsequent treatment with the anti-cancer drug 5-FU at different concentrations (0.0 mM, 0.5 mM, 5.0 mM and 50.0 mM). The error bars denote the standard deviation as obtained from  $n = 3$  independent repeats, each repeat containing triplicates per concentration of 5-FU in question. For every condition, the data was normalized to the metabolic activity corresponding to 0.0 mM. Statistical significance was obtained by one-way ANOVA test by Prism 9.0. \*, \*\*, \*\*\*, and \*\*\*\* indicate  $p$  values of  $<0.0332$ , 0.0021, 0.0002,

and 0.0001, respectively. For LS174T vs L174T BSM, *p* values are 0.0154, 0.0013 and 0.0021 for 0.5, 5.0 and 50.0 mM of 5-FU, respectively. .... 55

Figure 3.8 Reorganization of data in Fgiure 3.7 to observe the behavior of no gel and BSM individually. The error bars denote the standard deviation as obtained from *n* = 3 independent repeats, each repeat containing triplicates per concentration of 5-FU in question. For every condition, the data was normalized to the metabolic activity corresponding to 0.0 mM. Statistical significance was obtained by one-way ANOVA test by Prism 9.0. \*, \*\*, \*\*\*, and \*\*\*\* indicate *p* values of <0.0332, 0.0021, 0.0002, and 0.0001, respectively. .... 55

Figure 3.9 Cell metabolic activity of HT-29, HT-29 MTX and LS174T either with hydrogel on the top layer or with BSM, and a subsequent treatment with the anti-cancer drug 5-FU at different concentrations (0.0 mM, 0.5 mM, 5.0 mM and 50.0 mM). The error bars denote the standard deviation as obtained from *n*=3 independent repeats, each repeat containing triplicates per concentration of 5-FU in question. For every condition, the data was normalized to the metabolic activity corresponding to 0.0 mM. Statistical significance was obtained by one-way ANOVA test by Prism 9.0. \*, \*\*, \*\*\*, and \*\*\*\* indicate *p* values of <0.0332, 0.0021, 0.0002, and 0.0001, respectively. At 5.0 mM of 5-FU in LS174T BSM vs LS174T alginate, the *p* value is 0.0075. .... 56

Figure 3.10 Reorganization of data in Figure 3.9 to observe the behaviors of BSM and alginate individually. The error bars denote the standard deviation as obtained from *n* = 3 independent repeats, each repeat containing triplicates per concentration of 5-FU in question. For every condition, the data was normalized to the metabolic activity corresponding to 0.0 mM. Statistical significance was obtained by one-way ANOVA test by Prism 9.0. \*, \*\*, \*\*\*, and \*\*\*\* indicate *p* values of <0.0332, 0.0021, 0.0002, and 0.0001, respectively. .... 56

Figure 3.11 Visual representation of the 3D model used in the drug resistance assay. In each well of a 96-well plate CRC cells were encapsulated in BSM or alginate. 5-FU was added at different concentrations for 24 h and a cell metabolic activity assay was carried out..... 57

Figure 3.12 Cell metabolic activity of HT-29, HT-29 MTX and LS174T following encapsulation in either BSM (A) or alginate (B) and a subsequent treatment with the anti-cancer drug 5-FU at different concentrations (0.0 mM, 5.0 mM and 50.0 mM). The error bars denote the standard deviation as obtained from *n*=3 independent repeats, each repeat containing triplicates per concentration of 5-FU. For every condition, the data was normalized to the metabolic activity corresponding to 0.0 mM. .... 58

Figure 3.13 Fluorescence microscopy images of MDR-1 expression in LS174T cells. CD44 is not shown here, but incubations with MDR-1 (Excitation/Emission of 590/617 nm) and CD44 (Excitation/Emission of 495/519 nm) antibodies result in membrane staining. Scale bar = 500  $\mu$ m..... 61

Figure 3.14 Mean fluorescence intensity quantification of MDR-1 in cells exposed to muc-gel (A) and alg-gel (B) for 6 h or 10 days. Quantification of CD44 in cells exposed to muc-gel (C) or alg-gel (D) for either 6 h or 10 days. The error bars denote the standard deviation as

obtained from  $n = 3$  images per condition using Cell Profiler software. Statistical significance was obtained by one-way ANOVA test by Prism 9.0. \*, \*\*, \*\*\*, and \*\*\*\* indicate  $p$  values of <0.0332, 0.0021, 0.0002, and 0.0001, respectively. LS174T 10 days, HT-29 6 h and LS174T 10 days conditions are not plotted, due to technical difficulties with the method used. Each mean intensity value corresponds to one object (spheroid)..... 62

Figure 5.1 Images taken under a bright field microscope to observe HT-29 spheroids encapsulated in BSM (A), alginate (B) as well as LS174T spheroids encapsulated in BSM (C) and alginate (D) hydrogels from day 0 to day 10 of encapsulation. Scale bars: 100, 200, 300 and 500  $\mu\text{m}$ , respectively. .... 3

Figure 5.2 The cytotoxic effect of the drug 5-FU in all three CRC cell lines. The first condition shows the cells before the drug treatment. The second condition shows the cells after a 24 h incubation with 50 mM of 5-FU. .... 4

Figure 5.3 Complete drug resistance assay performed on the 2D culture model in three different conditions: absence of gel, presence of BSM or alginate. 5-FU was administered at different conditions: 0.0 mM, 0.5 mM, 5 mM and 50 mM with a normalization to the control (0.0 mM). The error bars designate the standard deviation as obtained from measurements of  $n = 3$  independent experiments. Statistical significance was obtained by one-way ANOVA test by Prism 9.0. \*, \*\*, \*\*\*, and \*\*\*\* indicate  $p$  values of <0.0332, 0.0021, 0.0002, and 0.0001, respectively. .... 5

Figure 5.4 Fluorescence microscopy images of MDR-1 expression in HT-29, HT-29 MTX and LS174T cells in BSM and alginate. The cells were covered by each hydrogel for 6 h or 10 days and the immunofluorescence assay was performed following the removal of hydrogel from the monolayer of cells. Scale bar = 1000  $\mu\text{m}$ . .... 6

Figure 5.5 Fluorescence microscopy images of CD44 expression in HT-29, HT-29 MTX and LS174T cells in BSM and alginate. The cells were covered by each hydrogel for 6 h or 10 days and the immunofluorescence assay was performed following the removal of hydrogel from the monolayer of cells. Scale bar = 100  $\mu\text{m}$ . .... 7





## ACRONYMS

<b>Alg-gel</b>	Alginate hydrogel
<b>BSM</b>	Bovine Submaxillary Mucin
<b>CRC</b>	Colorectal cancer
<b>EDC</b>	1-ethyl-3-(3-dimethylaminopropyl)-carbodiimide
<b>EGF</b>	Epidermal growth factor
<b>Muc-gel</b>	Crosslinked BSM hydrogel
<b>Nb</b>	Norbornene
<b>NHS</b>	N-hydroxysuccinimide
<b>SEA</b>	Sea urchin sperm protein, enterokinase, agrin
<b>Tz</b>	Tetrazine
<b>5-FU</b>	Fluourouracil

# INTRODUCTION

Mucins exhibit fascinating purposes in the human body and can be engineered in materials that mimic or enhance these functions to solve challenges in the biomedical industry. A 3D model with a relevant mucinous tumor microenvironment that could accurately reproduce the *in vivo* situation, would be a step forward towards developing more reliable *in vitro* models for cancer research. Among other advantages, this would be beneficial for drug screening and reducing animal experimentation [1].

## 1.1 Mucins as the major protein component of mucus

Mucins are high molecular weight glycoproteins found in the cell membrane, being expressed as membrane-associated proteins anchored to the apical cell surface, or covering the wet epithelial surfaces in the form of mucus gel, as a result of being secreted by goblet cells of the epithelium [2]. The MUC gene family counts with more than 20 mucin genes which are named according to their order of discovery and organized based on the previously mentioned classification. For example, MUC1, MUC3A, MUC3B and MUC4 are membrane mucins, whereas MUC2, MUC5AC and MUC5B are secreted mucins [1], [3]. Furthermore, secreted mucins can be distinguished in large gel-forming mucins (MUC2, MUC5AC, MUC5B, MUC6, MUC19) or small soluble mucins (MUC7, MUC8, MUC9) [4].

Gel-forming (secreted) mucins are entirely extracellular, forming a mucus layer on epithelial surfaces and providing mucus with its viscoelastic properties. This three-dimensional network is achieved via oligomerization domains to protect underlying epithelia against various offences, such as inflammation, bacteria, virus, pH, pollutants, etc. On the other hand, membrane-associated mucins are bound by a transmembrane domain and manifest the molecular composition of the cell surface [5]. This can be done by different kinds of interactions, such as pathogen binding and cell adhesion, as well as intracellular signal transduction (e.g. MUC4 interferes with ErbB2, a growth factor receptor associated with human cancers) [6], [7].

Secreted mucins are the “classical” type of mucins and the key element in the context of this project. The biosynthesis of mucins starts in the endoplasmic reticulum. There, the peptide core is translated, the cysteine rich N and C terminal domains are folded, hence forming intracellular disulfide bonds, and N-glycosylation takes place. Before leaving this organelle, the mucin peptides dimerize and proceed to the Golgi apparatus, where serine and threonine residues are heavily O-glycosylated. Following the elongation of O-linked oligosaccharides and polymerization of mucins to form linear and branched polymers, these are stored in vesicles with  $Ca^{2+}$  [8]. It is thought that calcium has a stabilizer effect by

shielding terminal sugars that confer a negative charge to the molecule and encouraging mucin condensation by acting as ionic cross-linkers. But, whenever stimulated (e.g contact of an enteric pathogen with the cell surface), mucin-producing goblet cells secrete the mucin vesicles through exocytosis, releasing their content in the extracellular space and swelling exceptionally: 100 to 1000-fold [9]. At last, the mucus gel network is formed. The continuous secretion of mucus preserves the mucus layer that has an immense importance as previously stated [4], [10].

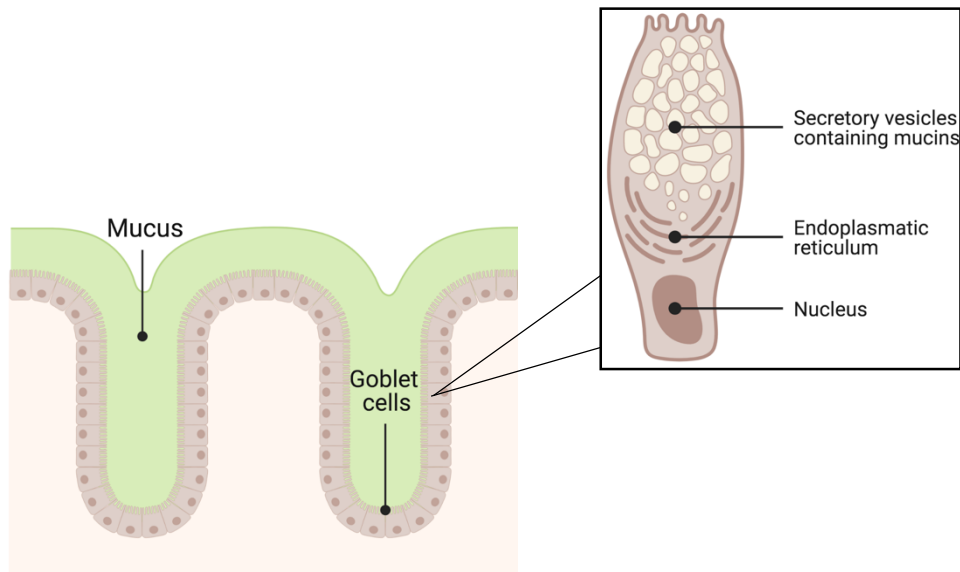


Figure 1.1 A representation of the colon epithelium with a mucus layer surrounding goblet cells- the main mucus producers in the human body. Specification of key constituents of goblet cells that participate in the production of mucus. While membrane mucins are cleaved into two subunits in the endoplasmic reticulum, inserted into the membrane and *N*-glycosylated, secreted mucins are *N*-glycosylated in the endoplasmic reticulum and dimerize via their C-terminal domains. Both types of mucins are *O*-glycosylated in the Golgi apparatus. Subsequently, the dimers of the secreted mucins undergo N-terminal oligomerization and are loaded into secretory granules. Other non-mucin molecules might form non-covalent interactions with mucins [24].

Covering the surface of many epithelial cells, mucus is primarily constituted of water (90-95%), providing a solvent and diffusion medium for salts, lipids and proteins between the extra- and intracellular milieu. Although both the ionic composition and the interactions with lipids are relevant for mucus gel to perform its functions of optimal protection, mucins are the preeminent functional component of the mucus, taking up approximately 3% of its composition [8].

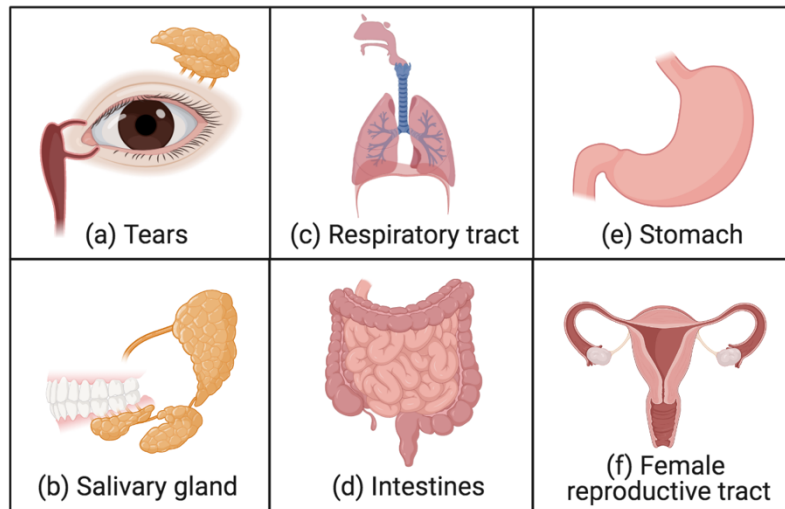
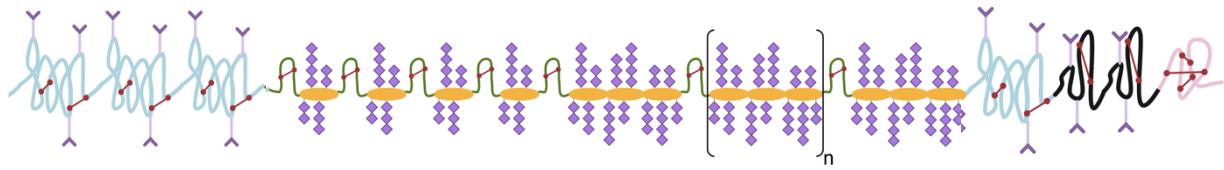


Figure 1.2 An overview of human mucosal surfaces, where mucus protects the epithelial cells through its barrier, hydrating/lubricating and bioactivity effects. The eyes take advantage of a microbial defense system characteristic of mucosal surfaces, and tears contribute with their antimicrobial components (a) [2], [119]. The salivary glands protect against the endless exposure to pathogens in the mouth by secreting antibodies that bind to the mucus layer of the epithelia in the oral cavity (b) [120]. In the respiratory tract, the mucus layer confines potentially dangerous external agents (e.g. pathogens, other particles) and contains cytokines that affect mucus secretion and immune cell activities in case of a respiratory infection (c) [121]. The gastrointestinal mucus layer not only acts as a physical barrier from external agents, but also provides lubrication/hydration in the lumen against adverse environments (e.g. gastric acid and digestive enzymes in the stomach) (d),(e) [122], [123]. Cervical mucus has a barrier effect against infections and also functions as a lubricant during sexual intercourse (f) [124].

Independently of their classification, all mucins share structural and compositional features: the apomucin core that comprehends around 20% (w/w) of the mucin mass and tandem repeats, namely proline, threonine and serine (PTS) sequences in the centre of the mucin protein backbone. For this reason, the long protein core has a tendency to exhibit densely O-glycosylated regions that account for 50-80% (w/w) of the carbohydrates. This is prompted by the fact that O-linked glycosylation usually occurs on amino acids with active hydroxyl groups, such as serine and threonine [8], [11]. Regarding proline, it was studied that there is an increased number of this amino acid around the glycosylated Ser/Thr when comparing with non-glycosylated sites [12]. There are multiple options when it comes to the terminal sugars displayed on the O-linked glycan, some of them attiring the mucins with a negative charge, including sialic acid sugars, *N*-acetylglucosamine, galactose and sulfate [13], [14].

Finally, it is equally worth noting the cysteine-rich regions of the protein core, in which N-glycosylation in carboxy- and amino- ends can be found. In the elongated gel-forming mucins, apart from these cysteine-rich regions that contribute with intra- and inter-molecular disulfide bonds and provide flexibility amidst the tandem sequences, there are Willebrand Factor D (vWF-D), vWF-C and carboxy-terminal cysteine knot (CTCK) domains. To simplify, these assist the assembly mechanism of mucins (oligomerization) to form linear polymers as illustrated in Figure 1.3 [15], [16].









Mucin domains					
Non- Glycosylated				Glycosylated	
					
vWF D	Cys rich	vWF C	Cys knot	Ser Thr Pro Repeats	O-linked Oligosaccharide

Figure 1.3 Illustration of gel forming mucin's structure. The extended protein core accommodates two regions: a central hydrophilic region with PTS tandem repeats, thus heavily O-glycosylated and the hydrophobic terminal regions that are sparsely N-glycosylated. As a result, the high-density glycosylation areas that cause mucins to have a negative charge provide a "bottle brush" arrangement of the oligosaccharides. This is due to the resulting steric hindrance of large molecules and charge repulsion between the glycoconjugates which simultaneously increase the stiffness of the molecule. Meanwhile, the less glycosylated areas that can either be in between PTS repeats or in the –N and –C terminals, display cysteine-rich regions and other disulfide-rich domains, namely vWF-D, vWF-C and cysteine knots. Therefore, mucins monomers assemble into dimers and then oligomers, which interact with each other via intermolecular bonds and entangle into a hydrogel previously referred to as mucus gel [4], [125], [126].

To summarize, the common characteristics to all mucins described here are the PTS tandem repeats that serve as sites for O-glycosylation, the extended central protein core- usually greater than 5,000 amino acids in gel forming mucins- that acts as a scaffold for the latter and the terminal acid sugars which influence the net charge of the molecule. Yet, there is variability concerning each mucin gene either in sequence, number of amino acids per tandem repeat or even the number of tandem repeats per allele itself. Heterogeneity of the oligosaccharides structure is also a factor to consider since the biological activity can be affected by glycosylation. This indicates an evolution of mucins to carry out specific functions depending on the organ in which they are expressed [17]–[19].

### 1.1.1 Properties of mucins

The substantial chemistry diversity involved in the mucin composition provides mucus with relevant properties. For instance, its hydration and lubrication, selective physical barrier and bioactivity by modulating cell behavior [20].

As shown in Figure 1.2, it becomes clear that the highly hydrated mucus gel covering the epithelium is the body's first line of defense in a variety of organs. In fact, it creates a selective barrier because it is indeed permeable to gases and nutrients necessary for a normal cell function. Yet, the entanglement of mucin polymers into a mesh with restricted pore sizes allows the exclusion of chemical, enzymatic, microbial and mechanical insults, which often are too large to cross the mucus layer [4], [21]. Depending

on the organ and health of individuals, the mucus layer can range from 10 (eyes) to 700  $\mu\text{m}$  (intestine) and the pore size from 20 to 1800 nm [22]. Interestingly, the barrier effect demonstrated by the mucins constituting the hydrogel layer is not entirely physical, meaning that there is an additional mechanism to determine the passage of molecules or pathogens through the gel besides the size exclusion principle [23]. Actually, this semi-permeable gel can trap microbes as if having an affinity filter based on the interaction of molecules with mucins. On top of that, it can shelter other antimicrobial molecules which participate in the barrier effect by targeting the external threats or even strengthen the mucus barrier (e.g. increasing its viscosity) [24]. Mucin domains display clusters of O-glycans pointing in every direction (Figure 1.3), making the central protein backbone beyond reach to proteases and creating a glycan surface of clustered antigens [25]. Thus, one could interpret that mucin's properties of hydration and lubrication, barrier and bioactivity effects are not independent but rather interconnected.

In this line of thought, it is essential to deepen the comprehension of mucin's bioactivity, which has been associated to both membrane bound mucins and secreted mucins towards microbes and mammalian cells. For instance, membrane-anchored mucins are thought to be related in signal transduction pathways because of its EGF and SEA domains extracellularly but also its cytoplasmic tail. On the contrary, secreted mucins solely interact with other proteins extracellularly, given its lack of a trans-membrane domain. The mucus layer is not a static barrier, but a dynamic environment of biochemical signals and interactions capable of determining the outcome of the surrounding cells (Figure 1.4). Such interactions can be established directly if mucins act as ligands to cell surface receptors, or indirectly if there is an entrapment of bioactive molecules into the mucin gel network [26], [27].

The non-glycosylated protein domains of mucins stand by the bioactivity of mucin molecules considering that the mucin epidermal growth factor-like domain (EGF-like)- a cysteine-rich region often found in membrane mucins- can bind to EGF receptors that act in modulating development, migration and differentiation of cells [28]. The O-glycosylated domains too have proven to be bioactive, particularly the gastric tract mucins against the common stomach *Helicobacter pylori* infection. By inhibiting the synthesis of a major cell wall component of the microbes, the O-glycans have shown to perform as a natural antibiotic under this circumstance [29]. The immune system cell surfaces are furnished with a complex mixture of glycans that can be recognized by multiple glycan-binding proteins. As previously mentioned, sialic acid habitually terminates mucin's glycan chains. The Siglecs are a receptor family of sialic-acid-binding immunoglobulin-like lectins that have been hypothesized to nurture cell-cell interactions and modulate functions of cells in the innate and adaptive immune systems through glycan recognition. Moreover, the interaction between sialic acid and Siglec receptors has been studied and associated with the induction of anti-tumor responses [30]–[32]. There are commensal bacteria living in the outer mucus of colon [26]. Since mucins can provide them with a carbon source, the sugars sprout around the protein core. Still, there are also pathogenic bacteria capable of developing mechanisms to degrade and avoid mucus and overall disrupt its protective role [36–38]. In the colon, a double layer of mucus protects the epithelium from the bacteria flora flourishing in the lumen: a top loose layer where mucin-bacteria interactions occur and the bottom layer consisting in a sort of aseptic zone to protect the

epithelium. Such separation prevents inflammation and it is possible because of MUC2, an hyperglycosylated gel forming mucin. Among other potential studies, one could highlight the immunoregulatory signals triggered by the binding of MUC2 to intestinal dendritic cells [33].

Apart from mucin-cells interaction, the sequestration of molecules should be taken in consideration. Growth factors, cytokines, antimicrobial peptides (AMPs), trefoil factors and antibodies are also found co-localized with mucins. The specialized goblet cells that express unique antimicrobial peptides AMPs keep commensals in check and prevent pathogen invasion. To maintain intestinal homeostasis, intestinal epithelial cells assist in transporting IgA molecules into the intestinal lumen. Invasive bacteria may traverse the epithelium and reach the basolateral surface of the epithelial cells, where they will be identified by a collection of different toll-like receptors (TLRs), including TLR2, TLR3, TLR4, and TLR5. When epithelial cells are activated, they initiate an innate immune response by releasing chemokines and cytokines that attract circulating immune cells. Antimicrobial peptides may be expressed directly by epithelial cells in response to microbial penetration. Furthermore, epithelial cells can generate tissue repair cytokines to heal mucosal injury and stress. Intraepithelial phagocytes, mostly macrophages and dendritic cells, contain pattern recognition receptors (PRRs) and may reach the lumen side of mucosal surfaces to identify commensals or pathogens and present different antigens. When bacteria propagate via an epithelial break, antigen-presenting cells (APCs) in the subepithelium detect them instantly via PRRs and deliver antigens to resident T or B cells. In general, various innate immune recognition patterns train the following adaptive immune response by stimulating the production of unique cytokines [34], [35]. Recent advances in mucosal immunity have shown diverse functions for the IL-17 family of cytokines in various epithelial barrier surfaces. Although the family members' epithelial cell-immune cell cross-talk is crucial for the coordination of immune function against invading pathogens, disruption of this contact frequently leads to inflammatory tissue lesions and even promotes carcinogenesis [36]. In this sense, epithelial cells are increasingly recognized as an important component of innate immunity. Significant interest in epithelial cells as a source and responder to cytokines has revealed that epithelial phenotypes are adaptable, depending on the tissue's specific requirement. Significant evidence is shown that epithelial cells contribute fundamentally to inflammatory resolution and that the dynamic interplay between pathogens and host epithelial cells may best highlight epithelial cells' significant involvement in inflammation orchestration [35].

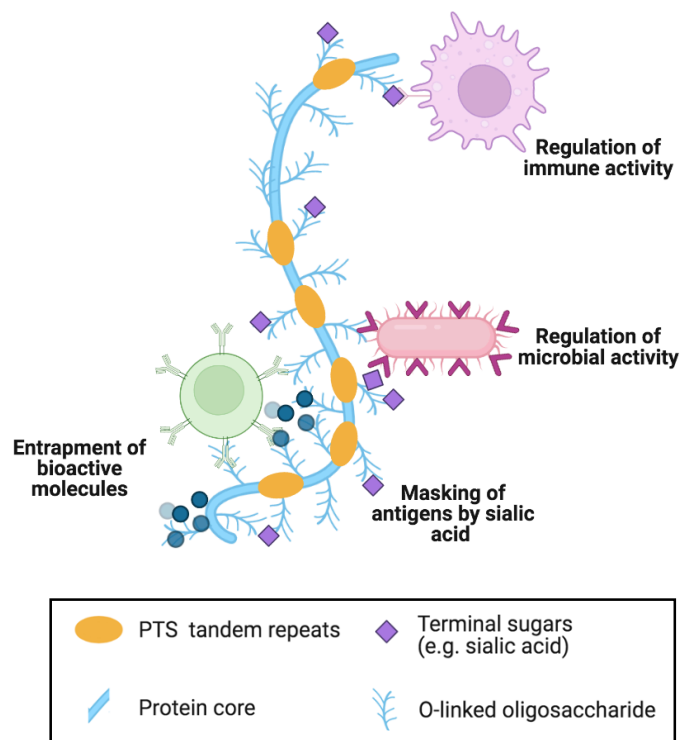


Figure 1.4 Representation of a mucin monomer to exemplify mucin’s bioactivity. On a larger scale, the mucus gel forms a physical barrier and prompts a multitude of biological responses from bacteria and mammalian cells, deconstructing the primordial idea that mucus consisted of a nonspecific static barrier. Both domains of the protein backbone and the terminal sugars of mucin glycans can operate as ligands. Distinctively, sialic acid residues are capable of shielding antigens from antibody recognition. Another type of interaction involves capturing bioactive molecules into the hydrogel mesh structure. Apart from immune cells, mucins influence bacterial behavior through biofilm formation, swimming and expression of virulence factors [22], [127].

### 1.1.2 Sources of secreted mucins and muc-gel

Mucin secretion is exclusively attributed to columnar epithelial cells [37] and it is indeed possible for these secreted mucins to be gel-forming, given the intermolecular crosslinking by noncovalent bonds. Along this thought, human colorectal carcinoma cell lines such as LS174T HT29-MTX and HT-29 have been used in this project for they mimic the altered glycosylation found in tumors *in vivo* [38], [39]. These epithelial cells contribute with the relevance of its secreted mucins while helping to retreat from animal-derived mucins. Nonetheless, the gels they form are weak *in vitro*. Among other animals, pigs and cows are typical mucin sources to employ as a building block for mucin-based biomaterials. With different organisms and tissues come distinct features on the protein sequence level, i.e. size, glycosylation degree, and the presence of domains such as Von Willebrand or cysteine rich areas [40]. Glycosylation, length, and structure are much more susceptible to change. To give an instance, pig gastric mucins contain more extended glycan chains, yet fewer terminal sialic acids than bovine submaxillary mucins [41]. The extraction *per se* can be done by collecting the mucus and extracting the mucins or by homogenizing whole tissues. Then, the purification process takes place by leveraging the rich chemistry of



mucins, that is its solubility profiles in solvents, large size and strong net negative charge. Contrarily to the glycosylated areas of mucins, the non-glycosylated sections are more accessible to proteolytic degradation [42]. To avoid disturbance of gelling properties of gel-forming mucins by proteolytic degradation, these can be purified by using a settled protocol of gentle water dissolution, size exclusion chromatography and cesium chloride density gradient centrifugation to remove mucin-bound impurities [43].

Bovine submaxillary mucins (BSM), abundant in well-known cancer markers Tn and Sialyl-Tn glycosylations, consist in a good approximation of abnormal colorectal carcinoma sugars in mucin molecules [44]–[46]. Therefore, BSM extracted from the salivary glands of cows as a by-product for food production were used as well to study mucin's influence in the situation of human mucinous tumors. Such material allows the development of robust cancer mucin hydrogels through a method of covalent crosslinking as supported in previous studies [13], [47]. Following the grafting of Tz and Nb amine derivatives on the activated carboxylic groups of mucins (BSM), the inverse electron-demand Diels-Alder reaction occurs between BSM-Nb and BSM-Tz and allows their covalent crosslinking once mixed. This consists in a "click chemistry" biorthogonal reaction, a concept created by Carolyn Bertozzi to define two-step chemical reactions requiring two functional groups with minimal impact on the biology itself. Primarily, the bioorthogonal functional moiety (chemical reporter) of a compound is incorporated into a substrate. Secondly, the reporter is covalently linked to an exogenous probe through a click reaction [48]. The Diels-Alder reaction happens by cycloaddition, meaning that in an uncomplicated reaction, a 1,3-diene and alkene(dienophile) yield a substituted cyclohexane ring, in which the electrons are transferred in a cyclic way between the diene and the alkene for the cyclic structure [49], [50]. Producing an insubstantial amount of diastereomers, it can be seen as a very productive reaction too. The bio orthogonality, biocompatibility, efficiency and specificity of this chemical reactions provide an opportunity to address emerging biomedical challenges [51]. Whilst in a complex biological environment the biomolecules can be studied in their native environments by virtue of this type of chemistry, without requiring toxic heavy metal catalysts [52].

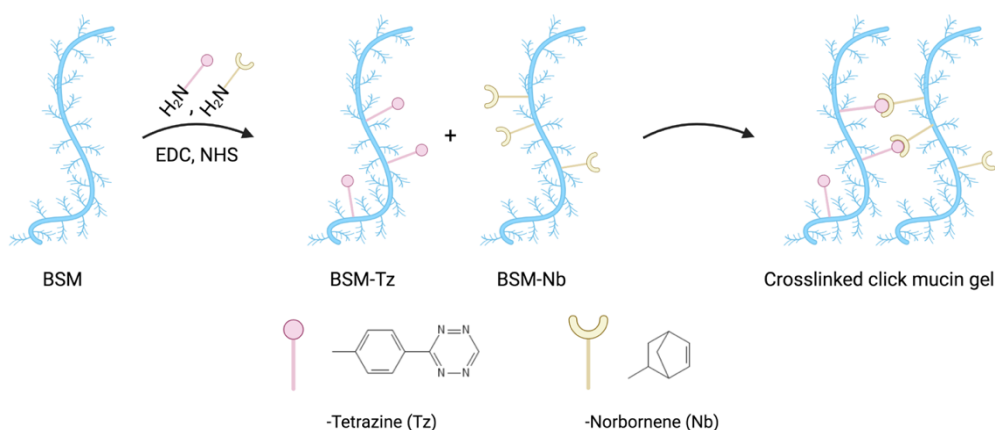


Figure 1.5 Representation of mucin modification following the EDC/NHS coupling and grafting of amine derivatives –Tz and –Nb on the mucin's protein backbone. Subsequent crosslink into a stable hydrogel when mixed due to the "click chemistry". The biorthogonal click reaction is specific and irreversible.

It is highly likely to recognise differences in disease states of the epithelium and in the composition and activity of the microbiota, which consequently can modify the glycan composition. On that note, it is essential to acknowledge batch to batch variability, an undeniable obstacle of working with animal tissues. Nevertheless, the general crucial characteristics of mucins are conserved, i.e. an extended central protein core, regions of dense O-glycosylation, and the presence of acidic sugars providing an overall negative charge to the molecule. So, the barrier, hydration & lubrication, and bioactivity functions can still be challenged [53]. In this project, the barrier and bioactivity properties have been brought into focus. In order to assess the viability of CRC cells encapsulated in muc-gel to mimic the mucinous carcinoma microenvironment, alginate hydrogels were used as a reference material. Given the resemblance to the environment of the natural soft tissue, hydrogels are promising in the biomedical field. Particularly, alginate hydrogels extracted from algae, have innumerable scale applications as food texturing agents, drug encapsulation material, and others. This reference gel was synthesized according to the same click chemistry principle as the muc-gel, acquiring stability and similar physical properties that canonical covalently crosslinked alginate hydrogels do not have. In fact, the latter lack of chemo selectivity, hence being potentially harmful to biological systems [54], [55].

## **1.2 Mucin-related diseases**

In practice, mucus' functions can be described by two principles: (a) Renewing the surface by continuously secreting goblet cells and washing away debris and (b) Protecting the surface by mucus coating. For cleaning, the mucus is key as its bioactive properties help to bind and gather debris- including pathogens- that are then carried away by a liquid flow on account of the hydrating and lubricating features of mucus. For protecting, mucus has to be adhered to the epithelial cells to remain and act as a coat. Under normal circumstances, the respiratory tract is cleaned by washing, while the colon is protected by a mucus coating. Depending on the obstacles, the majority of organs can switch between the two principles, a vital competence to study how the body works in health and disease [56]. In fact, many diseases are deeply connected to the influence of environmental factors (e.g pH, ionic strength, shear) on mucin's properties and to changes in the concentration of mucus and secreted mucins. To sustain this statement, it can be noted that in healthy conditions mucus protects the airways, although the upregulation of mucins and mucus overproduction actually relates to airway diseases, including cystic fibrosis, chronic obstructive pulmonary disease and asthma [57], [58]. The pH impacts mucin's conformational changes and concomitantly its viscoelasticity. Intriguingly, the aftermath of a viscoelasticity increase depends on the epithelium surface in question. It can translate into a benefit in the protection of the gastrointestinal tract or be detrimental in a disease state such as cystic fibrosis, in which a greater mucus viscosity is equal to a reduced mucociliary clearance- the self-clearing mechanism of the airways [59]. Meanwhile, the underproduction of mucus reflects other issues. For example, the resultant lack of lubrication in the eyes connected to dry eye disease [60]. Finally, and most importantly in the context of this thesis, it is understood that in many types of cancers mucins indicate differences concerning expression and composition [61]. Studying this biopolymer in the context of mucin-related

diseases such as colorectal adenocarcinoma will continuously allow to gain insights to develop accurate drug delivery systems.

### **1.2.1 Poor prognosis of CRC and aberrant mucin expression**

It is estimated that CRC is the third most recurrent cancer type and comes in second regarding the cause of cancer death worldwide. The International Agency for Research on Cancer (IARC) discloses that there are approximately 2 million new cases of CRC and almost 1 million deaths every year [62]. This type of cancer is usually classified as an adenocarcinoma (AC) and in 10-15% of cases as a mucinous carcinoma (MC), characterized by an excessive mucus secretion that comprises 50% of the tumor volume at the minimum. There are considerable clinical and histopathological differences between the two subtypes of CRC. It has been hypothesized that this is due to distinct molecular signatures and properties of MC comparing with AC. Having a poor prognosis, the progression, metastasis and treatment of CRC still represents a critical health burden in the medical field [63], [64].

Abnormal patterns of mucin expression are known to be related with multiple *neoplasias* [65]. MUC5AC and MUC6, normally absent in healthy mucosa, were identified in CRC progression, promoting cell invasion and migration and reduced apoptosis of CRC cells. Previous studies have also found an up-regulation of MUC2 in colorectal carcinomas and at least 50% of the tumor area having mucinous differentiation [66]. In fact, mucinous differentiation is associated with specific genetic and molecular features, namely CpG island methylator phenotype and microsatellite instability. The former is derived by an abundant expression of MUC2 and *de novo* expression of MUC5AC and the latter might be a result of genetic hyper mutability [3]. The paradoxical involvement of MUC2 in gastrointestinal tract malignancies as an inflammatory suppressor and a promoter of tumor initiation may imply that gastrointestinal tract cancers start from cells that express MUC2 rather than MUC2 itself having a role in the malignant process [67]. Contrasting with healthy epithelial cells, which secrete mucins under strict regulation, in tumors, there is a limited immune recognition of tumor cell epitopes caused by the physical and biochemical barrier of high density mucins at the membrane surface [14]. Moreover, altered glycosylation of MUC1 on tumor cells influences tumor initiation, progression, and metastasis as well as cancer immune surveillance, enabling cells to escape the immune response by expressing this transmembrane glycoprotein [68]–[70].

### **1.2.2 Chemotherapy effectiveness against mucinous tumors**

Previous studies have shown that maintaining the effectiveness of chemotherapy remains a challenge, often unsuccessful as in the case of pancreatic cancer. Particularly, a study showed a correlation between MUC1 up-regulation in pancreatic cancer and a limited success of the anti-cancer drug 5-Fluorouracil (5-FU). Similarly, up-regulation of MUC5AC observed in CRC patient tissues and cell lines resulted in resistance to 5-FU and oxaliplatin and its knockout increased sensitivity to these drugs. Despite its faulty selectivity, the 5-FU drug has antitumor activity. However, an appropriate amount of 5-FU must be converted intracellularly to its active form, to perform the desired cytotoxic effect. In other

words, 5-FU is converted to FdUMP and, subsequently, a complex between the latter and thymidylate synthase must be formed in order to inhibit DNA replication and repair. In cases of overexpression of mucins by tumor cells, such mechanism is hampered. Specifically, the general response rate for advanced CRC of 5-FU alone is only 10–15%, and in combination with other anti-cancer drugs it is 40–50%, which reiterates the urgency of breakthrough strategies for therapy [71], [72]. CRC cells' response to chemotherapy (mucin secretion) is comparable to epithelial cells' planned response to toxins or infections. Just like mucin-producing cells would produce enormous amounts of mucins to separate themselves from the insults (toxins, allergens, or infections) in this disease-state, a barrier against the treatment is also created. An intriguing topic is how the combination of 5-FU + irinotecan stimulated mucin production and rose the question regarding a potential receptor or intracellular pathway that is triggered by these substances. This observation is significant in the use of chemotherapeutics and warrants additional research [67].

The resistance to chemotherapy observed through imaging-based technologies, namely computed tomography and positron emission technology, is a serious challenge and highlights the importance of personalized treatments for patients, considering their tumor genomes. When in pathological states, the epidermal growth factor receptor (EGFR) is well known for its role in tumorigenesis, which can be manifested through point mutations and transcriptional upregulation in breast, colorectal and lung cancers. Remarkably, in 2004 the FDA approved cetuximab, capable of blocking the epidermal EGFR activity [73], [74]. For some time, it was thought that targeted therapies such as the one mentioned would not be efficient in tumors with RAS mutations, regardless of which small G protein was affected (KRAS, NRAS or HRAS). However, there was an improvement of drug options for CRC patients, according to a recent study from the Salk Institute. In a normal scenario, RAS proteins are tightly controlled acting as binary switches (on/off states) in cell signaling. On the other hand, not only RAS mutations are indeed associated with oncogenesis, but also are the most frequent mutated gene in human cancer. Also, given their signaling role in diverse contexts, for example proliferation, oxidative stress, inflammation and drug resistance, it is plausible to hypothesize that RAS mutations have a different impact in CRC patients in terms of survival rate and resistance to cancer therapy [75], [76]. In this extensive work, researchers discovered ten different RAS mutations that do not limit the usage of EGFR inhibitors. Many of the medications that would be effective for these mutations are currently FDA-approved for other purposes [77], which could provide CRC patients with adequate treatment options. Regardless, the elements that contribute to the development of mucinous colorectal adenocarcinoma and their prognostic consequences are yet unknown.

### **1.2.3 Biomedical applications of mucins**

As aforementioned, several remarkable phenomena take place at the mucosa, making it a great candidate to explore tissue engineering, drug delivery, and hydrating & lubricating surfaces. Simultaneously, it constitutes a challenge when attempting to understand mucins interactions with the underlying tissue.

Due to immune modulating skills, mucins stood out and gave rise to various chances of leveraging its bioactivity in the biomaterials field. Implantation of biomaterials result in either fibrosis isolated biomaterials or fibrosis integrated biomaterials. Both innate and adaptive immune cells are involved in the immunological feedback to biomaterial implantation, with macrophages playing a key role since they respond non-specifically to an unfamiliar substance, whereas the adaptive immune system creates long-term immune memory to particular antigens. When investigating the immune modifying characteristics of mucins, macrophages and the innate immune response in general can establish the course of the early inflammatory actions [78], [79]. The Crouzier group engineered mucins and showed that muc-gels diminished macrophage activation when comparing to alginate hydrogels that have long been used in the field. Muc-gels deceived fibrosis after implantation in mice, proving to be a potential encapsulation material for cell and micro tissue transplantation. An elegant proposition made by the Crouzier group to boost this biomedical application consists in taking advantage of the click chemistry involved in the muc-gel system, by using non-crosslinked –Tz and/or –Nb to include growth factors. Thus, a better engraftment of the transplants could be achieved as a consequence of cell growth and differentiation stimulated former to transplantation [13], [68].

It is mandatory to consider the physical barrier effect of mucins and the meaning of inherent interactions (e.g. the transport of microbes) when approaching the design of effective drug delivery to the underlying epithelium. Drug carriers can be purposefully tailored to stick to or penetrate the mucus layer so it is critical to evaluate the possible impact of compromising the integrity of the mucus gel- namely exposure of the underlying tissues to bacteria, virus and other external particles- while assessing efforts to permeabilize the mucus barrier [80]. With the intent to re-establish healthy mucus, strategies to weaken or strengthen- depending on which mucus components are modified- have been developed *in vivo*. Said modifications can either be structural if, for instance, it involves pore size alterations in the network or related to the composition of mucus, if it affects mucin's concentration and/or glycosylation, for example. Natural occurring or purposefully induced stimuli can be behind these alterations, not forgetting the potential abnormal phenomena in disease-states. On the one hand, the binding of factors to mucus components may result in an augmentation of mucus cross-links and viscosity, stimulation of protein secretion, and/or inhibition of pathogenic population in the epithelium. On the other hand, enzymes secreted by the host, viruses, and microbes can break down the mucus layer by cleaving oligo-saccharides or the mucin protein backbone, disturbing inter- or intramolecular interactions, hence decreasing mucus viscosity [81], [82] (Figure 1.6).

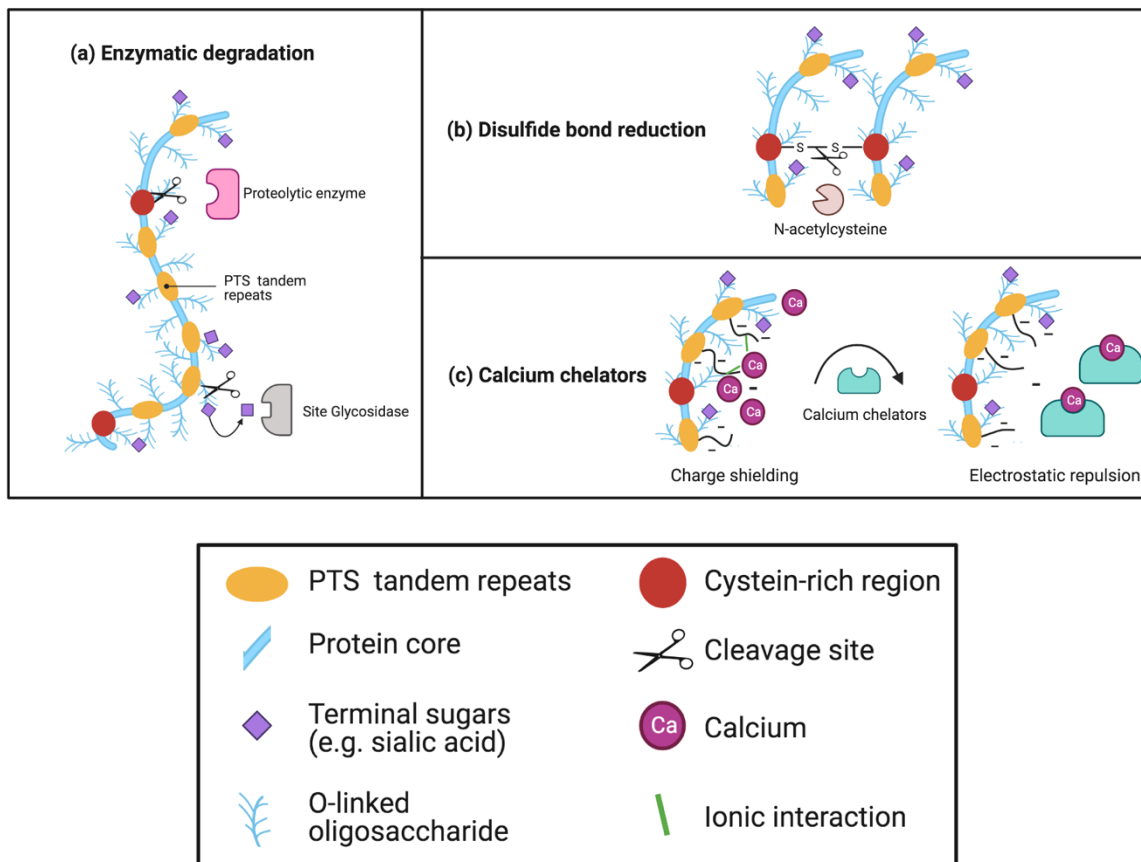


Figure 1.6 Scheme of methods to break down the mucin structure, weakening its barrier effect. As earlier mentioned, the non-glycosylated domains are an easy target to proteolytic enzymes, which can cleave peptide bonds. Once proteins are damaged- the mucin protein backbone or any other proteins in the gel- the permeability of the mucus gel is raised (a) [80]. An alternative to deal with mucus over-production is to resort to chemical agents, namely mucolytics, expectorants and mucokinetics that affect mucin polymerization [128]. N-acetylcysteine (NAC) is an example of a mucolytic with an effect on the mucins crosslinking. It reduces the disulphide bonds responsible for connecting mucin monomers into dimers, multimers etc, hence decreasing mucus viscosity and enlarging the pore size of the mesh [129]. Then, the diffusion of particles is facilitated, which is crucial in diseases characterized by a critical airway obstruction, as cystic fibrosis (b) [130], [131]. Lastly, calcium chelators can be added in order to alter mucin crosslinking. Calcium is vital in providing cationic shielding to maintain negatively charged mucins condensed and securely packed within goblet cell mucus granules. Thus, the process of chelating  $Ca^{2+}$  from mucus is responsible for a fast swelling of the gel and consequently, a more disperse, fluid and hydrated network of mucins (c) [82], [132].

Contrastingly, other agents have the ability to strengthen the properties of mucus and can even affect mucin's interactions. One example could be the lipids and salts inherently found in mucus and food, which is confirmed by experiments targeting particle diffusion through mucus. Alterations in the mucus layer may cause microbial invasion and inflammation due to exposure of the epithelium. Other studies have indicated that food intake significantly alters the environment in the GI tract, in light of the fact that it impacts pH, increases  $Ca^{2+}$  concentration, changes the ability of particles to reach underlying epithelium, and mucus structure [83]. Lower pH following the secretion of stomach acid increases gastric mucin's viscosity, whereas calcium ions are thought to aid the assembly of mucins into large aggregates [84], [85]. To a great degree, eating transforms composition, transport rates and production of mucus

and the resulting stimuli, e.g. lipids, have been shown not only to change the mucosal barrier, but also hinder the transport of model drug carriers through mucus. This suggests that alterations in the mucus layer caused by oral ingestion of lipids might assist in the protection of the underlying epithelium from exposure to ingested particulates [86]. Oral nutrient and drug delivery depends on the diffusion efficiency through mucus so it can subsequently enter the circulatory system. Whereas the barrier effect of mucus can indeed protect the epithelium, its complex modulation by physiological factors ought to be examined. Thus, researchers can pursue an effective design of oral therapies and skilfully explore mild stimuli for modulating intestinal mucus to expedite drug delivery [83].

Overall, mucin's properties are a powerful starting point to design new therapies and treat mucus-related diseases. Perpetuating research with respect to the mechanisms by which mucus demonstrates its bioactivity through a myriad of interactions, its effective barrier and mechanisms by which this barrier might be modulated will certainly encourage elegant approaches for engineering this natural hydrogel to be of service to health and attenuate disease. The natural extracellular matrix (ECM) not only acts as a framework for organizing cells into tissues, but it is also a rich source of stimuli that influence cell fate decisions [87]. The mechanics and chemistry of the ECM both influence cellular activities including migration, proliferation, and differentiation can be modulated by the mechanics and biochemistry of the ECM. Building adjustable synthetic ECMs is a bright approach to control cell phenotypes for applications in tissue engineering, regenerative medicine, and *in vitro* disease models [88], [89]. The natural ECM is a water-swollen network composed primarily of proteins and polysaccharides. Hydrogels having natural polysaccharides in its composition, natural and engineered proteins, and synthetic polymers have been utilized to encapsulate cells for 3D culture and transplantation in order to imitate the features of the ECM.

To be considered an appropriate platform for cell encapsulation, hydrogel crosslinking and functionalization chemistry must be compatible with living cells. Many methods for 3D cell encapsulation utilize covalent crosslinking reactions instead of physical crosslinking. The main reason behind that consists in the greater stability provided by covalent bonds. Consequently, matrix properties are maintained over time and can normally achieve a higher range of material stiffness [90], [91]. The design of a hydrogel ECM mimics for cell encapsulation requires special attention in terms of potential off-target effects of the crosslinking methods. The best fitting gelation chemistry would be bioorthogonal to diminish the possible misleading effects of hydrogel crosslinking events on cellular phenotype, e.g interactions between chemical crosslinkers and functional groups in cell-surface proteins. Bioorthogonal reactions are those that involve chemical reaction pairings that (1) do not occur naturally in biological systems, (2) do not cross-react with functional groups found in biology, and (3) do not need or create cytotoxic byproducts [92], [93].

This project aimed at developing a new *in vitro* model of mucinous tumors, i.e tumors producing mucus protective encapsulations, while considering the 3 Rs principle of ethics in animal experimentation- replace, reduce, refine. The model consists in colonic cancer cell lines, embedded in new mucin-based covalently crosslinked hydrogels. In a first stage, the cell lines were encapsulated in the mucin or alginate gels to verify that cell proliferation and growth was attainable. Secondly, an extensive drug resistance assay was performed on the 2D model composed of cancer cells covered with BSM or alginate gels, as a means to detect a protective effect of the hydrogels against the selected anti-cancer drug. Then, the cells were encapsulated in both gels separately (3D model) at different time points (6 h and 10 days), to look into potential phenotype developments that would increase drug resistance over time- possibly the involvement of a biological barrier too. Aligned with the last-mentioned hypothesis, an immunostaining assay was carried out to conclude about the expression of a multi-drug resistance protein, as well as a cancer stem cell marker.



## MATERIALS AND METHODS

All figures in this document were made with Biorender.com.

### 2.1 Mucin and alginate gels

#### 2.1.1 Synthesis of hydrogels

##### BSM hydrogel

The inverse electron-demand Diels-Alder reaction between BSM-Nb and BSM-Tz allows their covalent cross linking. This consists of a “click chemistry” biorthogonal reaction. The dry BSM (Sigma-Aldrich, M3895-500MG, Type I-S) were pre-dissolved in MES buffer (0.1 M MES, 0.3 M NaCl, pH 6.5) at a concentration of 10 mg/mL overnight at 4°C.

1-ethyl-3-(3-dimethylaminopropyl)-carbodiimide hydrochloride (EDC; Sigma-Aldrich) and N-hydroxysuccinimide (NHS; Sigma-Aldrich) were added at 4 mmol per gram of dry mucin to the previously dissolved BSM solution and stirred at room temperature for approximately 10 min. Once the mixture is split into two tubes, 5-norbornene-2-methylamine (Tokyo Chemical Industry and tetrazine-amine (BroadPharm) were added individually at 2 mmol per gram of dry mucin and 1 mmol per gram of dry mucin, respectively. Both solutions were stirred overnight at 4°C. Following the crosslinking reaction, the mixtures were dialyzed in 100 kDa MWCO dialysis tubing (SpectraPor® Float-A-Lyzer® G2) two days against 200 mM NaCl and one day against Mili-Q H<sub>2</sub>O. Then, the samples were freeze-dried and stored at -20°C.

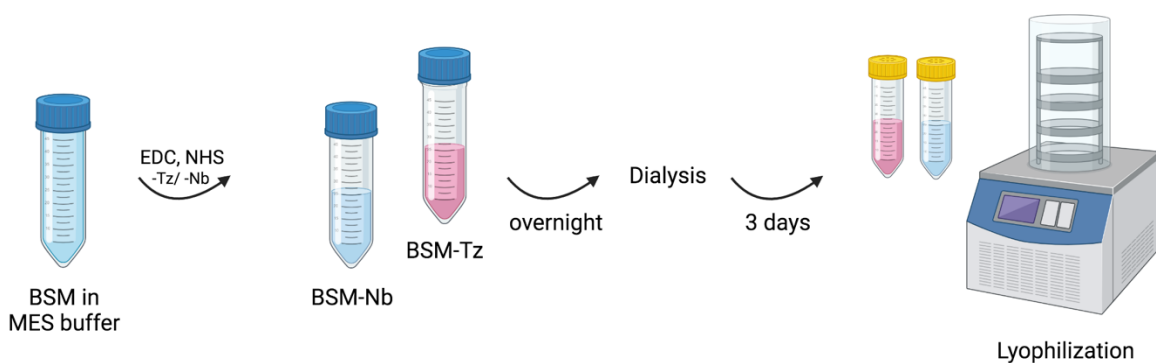


Figure 2.1 Schematic representation of the synthesis of BSM gelling components.

## Alginate hydrogel

The high molecular weight alginate (PRONOVA SLG20, NovaMatrix) was dissolved at 0.5% w/v in a 0.1 M MES, 0.3 NaCl pH 6.5 buffer. Then, N-hydroxysuccinimide (NHS; Sigma-Aldrich) and 1-ethyl-3-(3-dimethylaminopropyl)-carbodiimide hydrochloride (EDC; Sigma-Aldrich) were added in 5x molar excess of the carboxylic acid groups of the alginate. The click alginate polymer was modified with either norbornene or tetrazine at 1 mmol per gram of alginate to obtain alginate-norbornene and alginate-tetrazine, respectively. Both solutions were stirred overnight at 4°C. Following the crosslinking reaction, the mixtures were dialyzed in 100 kDa MWCO dialysis tubing (SpectraPor® Float-A-Lyzer® G2) two days against 200 mM NaCl and one day against Mili-Q H<sub>2</sub>O. Then, the samples were freeze-dried and stored at -20°C.

### 2.1.2 Rheological properties of BSM

The rheological properties of the mucin-gel were measured using a shear rheometer (MCR92, Anton Paar) containing a plate-plate measuring geometry (measuring head: PP50, Anton Paar, Graz, Austria). The gap between the measuring head and the bottom plate was set to  $d = 0.15$  mm for all measurements. The functionalized gel-components were diluted separately in PBS (pH 7.3) to a concentration of 25 mg/mL. Immediately before the measurements, equal volumes of the two gel components were mixed, vortexed for 30 s. Then, a strain-frequency sweep ( $f_{\text{start}} = 10$  Hz,  $f_{\text{end}} = 0.01$  Hz) was conducted to assess the frequency dependent viscoelasticity of the crosslinked sample.

## 2.2 Human colorectal adenocarcinoma cells

### 2.2.1 Cell culture

The cell culture of LS174T, HT29-MTX and HT29 cell lines was carried out on adhesion T75 flasks, using DMEM/F-12 (1:1) (1X) + GlutaMAX medium (Gibco) supplemented with 10% Fetal Bovine Serum (FBS) and 1% penicillin/streptomycin (100 U/mL). The medium was changed 2 to 3 times per week. Sub-confluent cultures were split when reaching 80% confluence. The medium was aspirated and the cells were rinsed with a balanced salt solution (e.g. PBS, 5 mL). PBS was removed and the cell dissociation reagent was added (e.g. accutase, 3-5 mL for a 75 cm<sup>2</sup> flask) to detach cells from the plate. The cells were incubated at 37°C for 5 min. Then, the accutase solution was neutralized by adding complete cell culture medium. The cell suspension was then centrifuged at 200 g for 5 min and the pellet was re-suspended in fresh complete medium to carry on the cell culture. When a specific number of cells was required to carry out experiments, the cells were counted using a haemocytometer. Otherwise, the overall sub cultivation ratio was between 1:3 to 1:8 as recommended by ATCC.

### **2.2.2 Cell encapsulation in hydrogels**

The gelling components (BSM-Tz/BSM-Nb and Alg-Tz/Alg-Nb) previously synthesized and lyophilized were dissolved in complete cell culture medium at 25 and 20 mg/mL, respectively. Once mixed at equal proportions, the hydrogels are formed. LS174T, HT29-MTX and HT29 cells were detached from the T75 flasks similarly to the sub culturing protocol and counted using a haemocytometer. To reach the desired cell density per well, the exact volume of cell suspension was centrifuged at 200 g for 5 min. The supernatant was removed and the cell pellet was re-suspended in mucin-gel (BSM) or alginate-gel. After 1 h, 50  $\mu$ L of cell culture medium were added on top of each well. Every 2-3 days the wells were washed, the medium was renewed and a cell viability assay was performed to assess the health state of the cancer cells' spheroids. In addition, images of the spheroids were taken under a bright field microscope in order to quantify the diameter of spheroids throughout the 10 days encapsulation.

### **2.2.3 Cell viability assay**

LS174T, HT29-MTX and HT29 cells were detached from the T75 flasks similarly to the sub culturing protocol and counted using a haemocytometer. To reach the desired cell density per well ( $6,9 \times 10^4$  cells/cm<sup>2</sup>), the exact volume of cell suspension was centrifuged at 200 g for 5 min. The supernatant was removed and the cell pellet was re-suspended in mucin-gel (BSM) or alginate-gel. The spheroids were cultured in the gels for 10 days. Every 2-3 days the medium was changed following a washing step with PBS and alamar blue assay was performed. To this end, the cells were incubated for 4 h with the alamar blue reagent (Invitrogen) at 10% of volume of culture in the well to detect cell viability through fluorescence measurement. The fluorescence intensity of the cells was determined using a plate reader (CLARIOstar, BMG LABTECH).

### **2.2.4 Drug resistance assay**

LS174T, HT29-MTX and HT29 cells were detached from the T75 flasks similarly to the subculturing protocol and counted using a haemocytometer. Then, the cells were seeded on 96 well plates at an initial cell density of ( $6,9 \times 10^4$  cells/cm<sup>2</sup>), using DMEM/F-12 (1:1) (1X) + GlutaMAX medium (Gibco) supplemented with 10% Fetal Bovine Serum (FBS) and 1% penicillin/streptomycin (100 U/mL, Gibco) and incubated at 37°C in a humidified atmosphere of 5% CO<sub>2</sub>.

### 2.2.4.1 2D model

The cells were first incubated for 24 h to enable attachment and mucus production and then challenged with different concentrations of 5-FU. In order to determine the appropriate range of concentrations to use (F6627-5G; Sigma-Aldrich) in the 2D culture system, six different concentrations were screened (50.0 mM, 5.0 mM, 2.5 mM, 1.0 mM, 0.5 mM, 0.1 mM, 0.05 mM). For each cell line and for each concentration, the cells were prepared in triplicate.

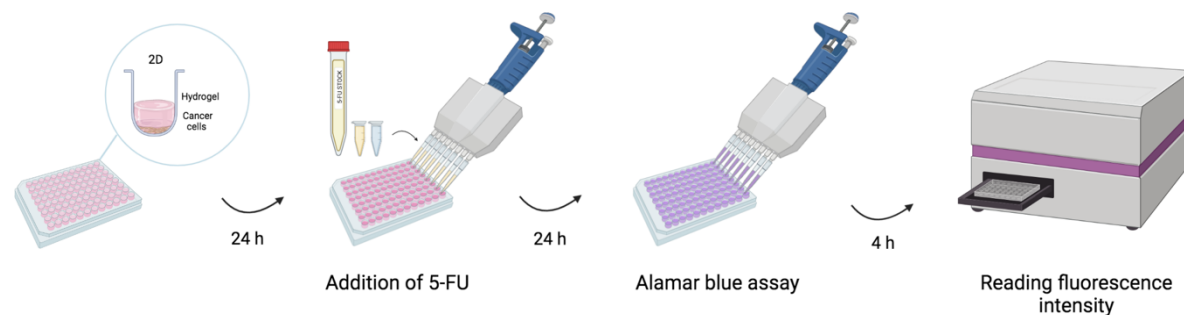


Figure 2.2 Schematic representation of the 2D model based on the seeding of cancer cells in the bottom layer of each well and a top layer of BSM or alginate covering the cell layer for 24 h. Subsequent administration of 5-FU to the cells and evaluation of cell viability.

Aiming to study the toxicity of 5-FU on HT-29, HT-29 MTX and LS174T cells, an alamar blue assay was performed. Following 24 h of exposure to 5-FU, HT-29, HT-29 MTX and LS174T cells were incubated for 4 h with the alamar blue reagent (Invitrogen) at 10% of volume of culture in the well to detect cell viability through fluorescence measurement. The fluorescence intensity of the cells was determined using a plate reader (CLARIOstar, BMG LABTECH).

### 2.2.4.2 3D model

The cells were encapsulated similarly to the method described in 2.2.2 and then challenged with different concentrations of 5-FU. Aiming to study the toxicity of 5-FU on HT-29, HT-29 MTX and LS174T cells encapsulated in BSM and alginate, an alamar blue assay was performed. Following 6 h or 10 days of exposure to 5-FU, the encapsulated cells were incubated for 4 h with the alamar blue reagent (Invitrogen) at 10% of volume of culture in the well to detect cell viability through fluorescence measurement. The fluorescence intensity of the cells was determined using a plate reader (CLARIOstar, BMG LABTECH).

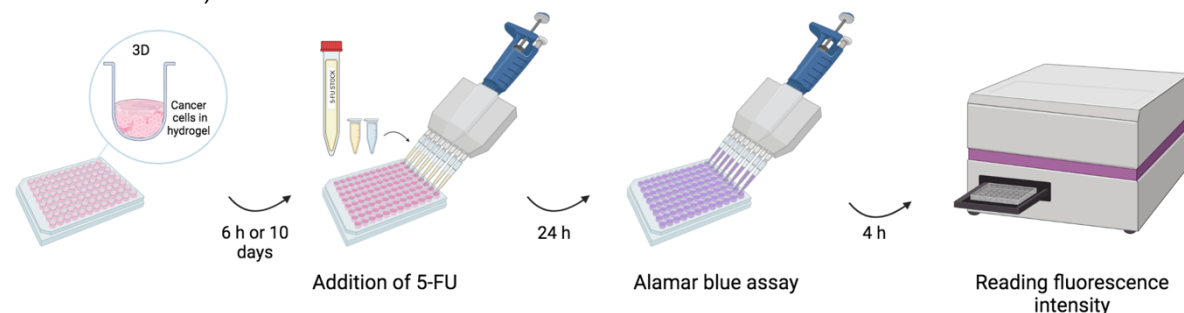


Figure 2.3 Schematic representation of the 3D model, consisting of cancer cells encapsulation in BSM or alginate for 6 h or 10 days. Subsequent administration of 5-FU to the cells and evaluation of cell viability.

## 2.3 Immunofluorescence

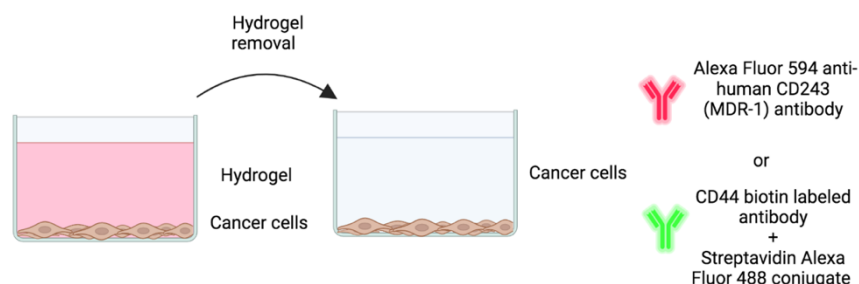


Figure 2.4 Illustration of the staining protocol conducted for the immunofluorescence assay in 8-well glass slides. The cells were seeded in a bottom layer, covered by a top layer of gel (BSM or alginate) similarly to the 2D model previously presented. After 6 h or 10 days, the top layer was removed to allow the staining of cells with antibodies, which otherwise would not penetrate muc- and alg- gels.

### 2.3.1 Staining cells for MDR-1

HT-29, HT-29 MTX and LS174T cells were individually seeded in 8 well glass slides (Millicell EZ SLIDE) at a density of  $3,7 \times 10^4$  cells/cm<sup>2</sup> with either alginate gel or mucin-gel covering the surface of the well. Prior to the staining protocol, the respective hydrogel was removed from the wells. For both time points, 6h and 10 days, the cells were firstly washed three times with phosphate buffered saline (PBS) and fixed in paraformaldehyde (4% w/v) in PBS for 30 min at room temperature (RT). Then, the samples were incubated for 1h at RT in PBS containing 5% (wt/v) bovine serum albumin (BSA) and washed three more times with PBS. Finally, the Alexa Fluor® 594 anti-human CD243 (MDR-1) antibody (BioLegend) was diluted at a ratio of 1:100 in PBS/ 1% BSA and added to the samples, which were incubated overnight at 4°C. The cells were counterstained with DAPI (4',6-diamidino-2-phenylindole) diluted at a ratio of 1:1000 for 5 min at RT and then washed with PBS 3 times. Lastly, the samples were visualized under a fluorescence microscope (Nikon Eclipse Ti-S).

### 2.3.2 Staining cells for CD44

HT-29, HT-29 MTX and LS174T cells were individually seeded in 8 well glass slides (Millicell EZ SLIDE) at a density of ( $3,7 \times 10^4$  cells/cm<sup>2</sup>) with either alginate gel or mucin-gel covering the surface of the well. Prior to the staining protocol, the respective hydrogel was removed from the wells. For both time points, 6h and 10 days, the cells were firstly washed three times with PBS and fixed in paraformaldehyde (4% w/v) in PBS for 30 min at RT. Then, the samples were incubated for 1h at RT in PBS containing 5% (wt/v) bovine serum albumin (blocking reagent) and washed three more times with PBS. The CD44 biotin-labelled antibody (BioSite) was diluted at a ratio of 1:100 in PBS/ 1% BSA and added to the samples, which were incubated overnight at 4°C. Then, labelled streptavidin was added at a ratio of 1:40 at RT for 1h and the cells were counterstained with DAPI diluted at a ratio of 1:1000 for 5 min at

RT. After washing with PBS 3 times, the samples were visualized under a fluorescence microscope (Nikon Eclipse Ti-S).

### **2.3.3 Spheroid size evaluation**

CRC spheroids embedded in BSM and alginate were used to determine spheroid size. This parameter was obtained by diameter measurement using Cell Profiler software. Results are expressed as mean ( $\mu\text{m}$ )  $\pm$  standard deviation.

### **2.3.4 Statistical Analysis**

Statistics analysis was determined by using GraphPad Prism 9.0 and \*, \*\*, \*\*\*, and \*\*\*\* indicate *p* values of <0.0332, 0.0021, 0.0002, and 0.0001 respectively, with a 95% confidence interval.

## RESULTS AND DISCUSSION

### 3.1 Click-chemistry of BSM with tetrazine and norbornene forms mucin hydrogels

A frequency sweep performed with the muc-gel (Figure 3.1) revealed a dominance of the storage modulus ( $G'$ ) from the beginning of the measurement, implying that a gel had formed. Indeed, previous time-sweeping rheology measurements of muc-gel samples done in the Crouzier group indicated a transition from a viscous solution (loss modulus dominated,  $G'' > G'$ ) to a viscoelastic gel (storage modulus dominated,  $G' > G''$ ) within 2-4 min. Moreover, a plateau state, in which the crosslinking reactions are approximately complete was expected within 40-60 min [13], [32]. Here, the frequency sweep was performed immediately after the transition between viscous and viscoelastic gel states, having reached a plateau of apparent efficient crosslink (Figure 3.1).

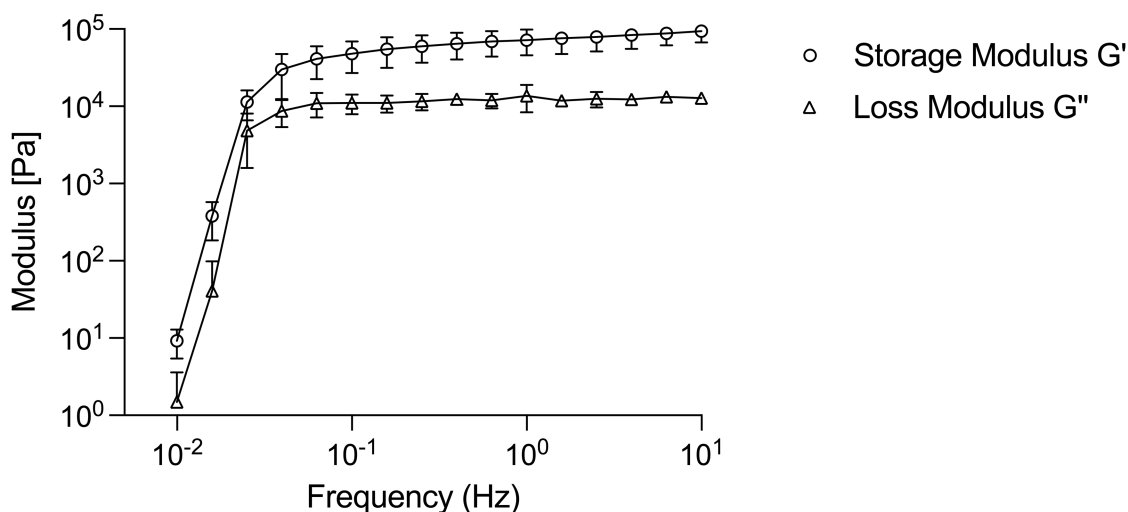


Figure 3.1 Rheological characterization of 2.5% muc-gels. Frequency-dependent viscoelastic behavior of muc-gels was evaluated by a rheometer. The error bars designate the standard deviation as obtained from measurements of  $n = 3$  independent experiments.

The inverse electron demand Diels–Alder cycloaddition reaction is a well received crosslinking mechanism for cell-encapsulating hydrogels and known to have rapid kinetics. However, the process of polymer crosslinking can be decelerated by steric hindrance of crosslinking sites on mucin peptide domains and electrostatic repulsion. By doing so, the access of proteases to the structure is restricted, avoiding its division into smaller fragments [32], [91]. Regarding the chemical synthesis itself, the reaction between tetrazine and other strained alkenes has been studied, and it was demonstrated that norbornene actually reacts slower with tetrazine than *trans*-cyclooctene (TCO). However, norbornene is way

more stable in solution and upon storage than TCO, mainly because of its *trans* double bond which can isomerize to the *cis* configuration in the course of time and accumulate in a non-reactive form [94]. All in all, the inverse electron demand Diels–Alder reaction is a valuable alternative for the synthesis of biocompatible hydrogels, circumventing certain limitations of ionically crosslinked hydrogels in 3D cell cultures and drug delivery *in vivo*. These limitations include poor crosslinking efficiency and faulty integrity of the materials [95]. The tetrazine/norbornene biorthogonal chemistry was applied to alginate by Joshi *et al.* [55], revealing a greater cell viability and cell metabolic activity than the ionically crosslinked hydrogel. The mechanical properties of hydrogels are fundamental when studying biomaterials and their outcome on the immune-mediated foreign body response (FBR). It has been suggested that stiffness of substrates might be involved in the foreign body response. In particular, poly (ethylene glycol) hydrogels modified with RGD prompt macrophage infiltration and fibrous capsule formation. Interestingly, the gravity of this foreign body reaction depends on the hydrogel stiffness. The lower the stiffness, the lesser macrophage activation occurs, as well as a more typical FBR [96], [97].

### 3.2 BSM and alginate support the encapsulation of CRC cells

All CRC cell lines under consideration were encapsulated for 10 days in both Muc- and Alg- gels to assess the health state and growth of the resulting cancer spheroids in the hydrogels in focus.

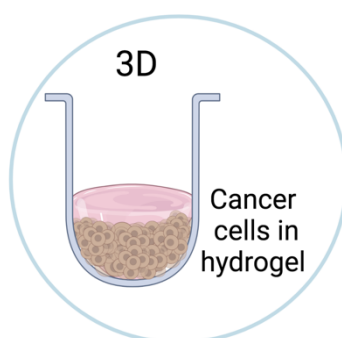


Figure 3.2 Visual representation of the 3D model consisting of CRC cells embedded in hydrogel (BSM or alginate) in 96-well plates.

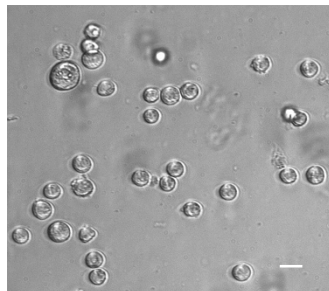
#### 3.2.1 CRC cells grow in BSM and alginate

Throughout the 10 days encapsulation of HT-29, HT-29 MTX and LS174T cells in BSM and alginate, the spheroids were observed under a bright field microscope and images were taken, in order to confirm its growth. Surely, the growth of CRC spheroids in the gels can be generally verified by the significantly difference of spheroids diameter between day 0 and day 10 of encapsulation in all conditions (Figure 5.1).

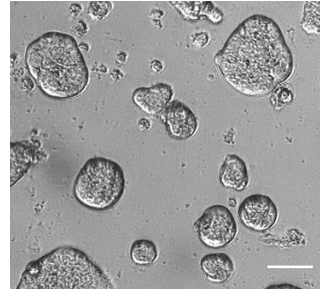


A

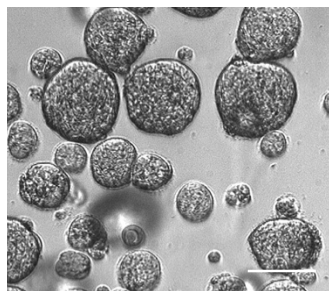
HT-29 MTX in BSM



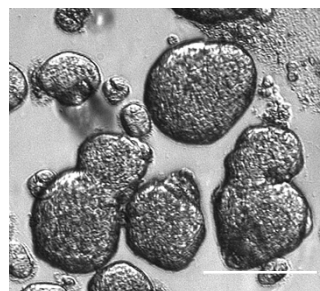
Day 0



Day 3



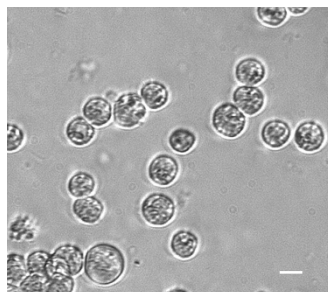
Day 7



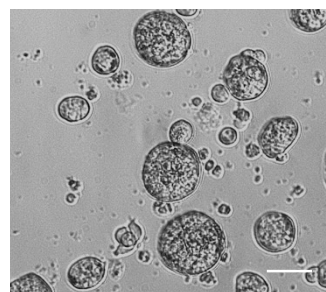
Day 10

B

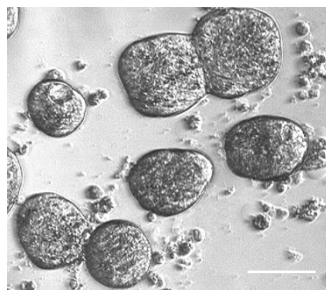
HT-29 MTX in alginate



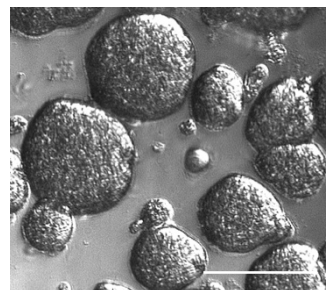
Day 0



Day 3



Day 7



Day 10

Figure 3.3 Images taken under a bright field microscope to observe the diameter of HT-29 MTX spheroids encapsulated in BSM (A) and alginate (B) hydrogels for 10 days. Scale bars: 100, 200, 300 and 500  $\mu\text{m}$ , respectively.

The diameter of HT-29 MTX spheroids in BSM exhibit a linear behavior of growth, with every time point revealing a significantly greater diameter than the previous time point. That in alginate could not be observed, only as a consequence of an insignificant difference of spheroids diameter between day 3 and day 7. As to HT-29 spheroids, the critical time points for diameter growth were seen from day 0 to day 3 in BSM and day 3 to day 7 in alginate. In the remaining instances, the growth was either insignificant- day 3 to day 7 in BSM and day 0 to day 3 in alginate- or there was an insignificant decrease in spheroids growth- day 7 to day 10 in BSM and alginate. Finally, for LS174T spheroids, its diameter significantly increased in BSM until day 7. In alginate, that only happened from day 3 onward. In BSM, HT-29 and HT-29 MTX had a 3-fold increase in diameter during the 10 days in gel, while LS174T had a 4-fold increase. In alginate, HT-29 had a 3-fold increase in diameter, HT-29 MTX had a 7-fold increase and LS174T had a 9-fold increase.

The plateau of growth observed is likely connected to certain limitations related to the culture of spheroids, as established by the work of others [98]–[100]. What initially consists in a proliferating mass of tumor cells rapidly transforms into a sphere characterized by proliferating cells in the periphery and viable, yet quiescent cells, in the inner core. During a final stage, the core becomes necrotic and the growth of cells in the periphery equals the cell death in the core. This could be due to diffusion limitations of nutrients, putting cells in a cell cycle arrest and essentially inhibiting spheroid growth [100].

Here, with respect to the moments of insignificant increase or decrease in the diameters, a further study for a longer period of time would be interesting to understand a bigger picture of diameter growth kinetics in these hydrogels and assess if the spheroids actually reached the size required for necrosis, which depends on various factors (e.g. initial cell seeding density, duration of experiments) and can start as early as day 8 for metastatic melanoma spheroids [101]. Another detail that could assist this goal would be to perform a daily evaluation or perhaps reduce the gap between each time point.

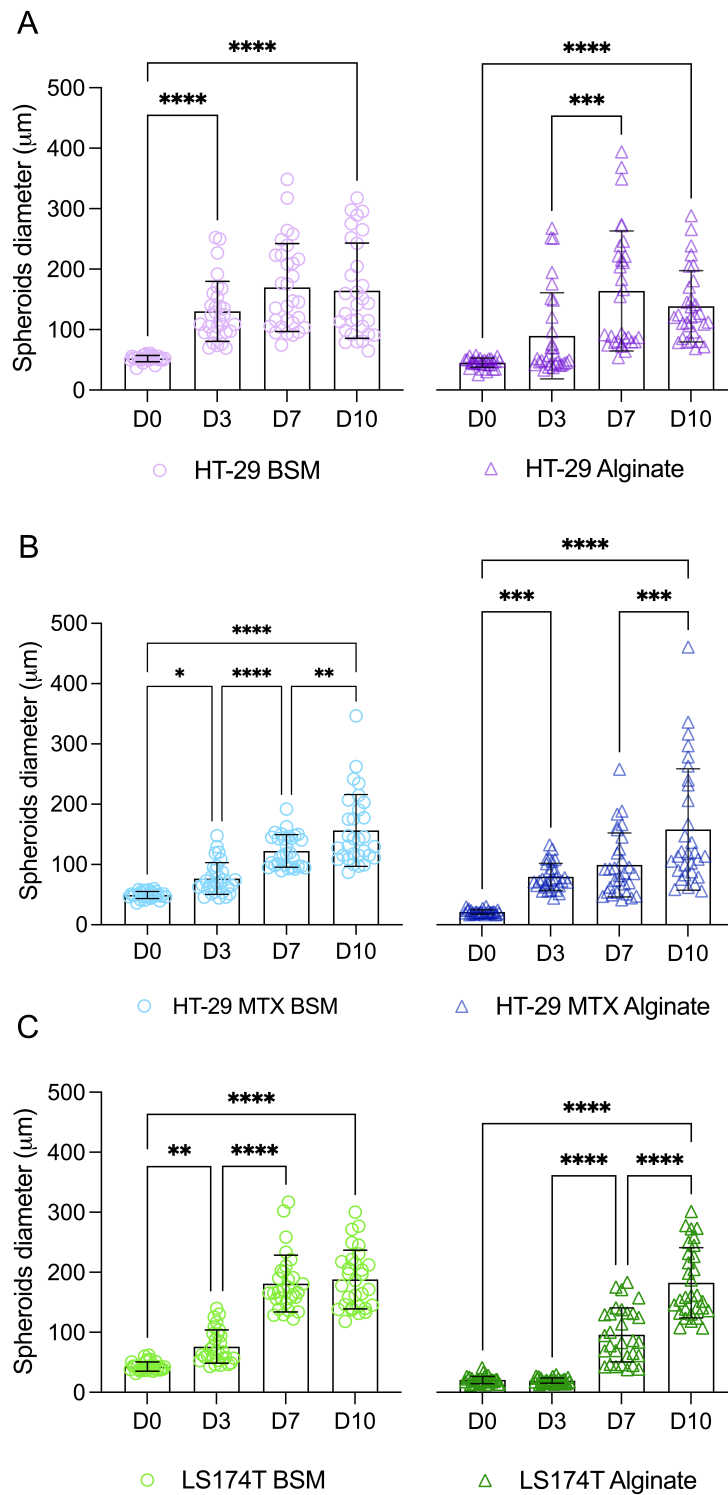


Figure 3.4 The diameter of HT-29 (A), HT-29 MTX (B) and LS174T (C) cancer spheroids encapsulated in BSM and alginate for 10 days was measured using the Cell Profiler software. Statistical significance was obtained by one-way ANOVA test by Prism 9.0. \*, \*\*, \*\*\*, and \*\*\*\* indicate  $p$  values of <0.0332, 0.0021, 0.0002, and 0.0001, respectively. The diameter quantification was done based on 18 images captured from  $n = 3$  independent repeats.

### 3.2.2 CRC cells are metabolically active in BSM and alginate

HT-29, HT-29 MTX and LS174T spheroids increased in metabolic activity during the 10 days encapsulation, with the exception of LS174T in alginate from day 1 to day 3. Although it is statistically non-significant, this time point revealed a decrease in metabolic activity. Under the same conditions in BSM, LS174T spheroids exhibited a non-significant increase in metabolic activity. Contrarily, from day 1 to day 3, HT-29 MTX was the only cell line showing a significant increase in metabolic activity both in BSM and alginate. From day 3 to day 7, the metabolic activity of HT-29, HT-29 MTX and LS174T spheroids became significantly greater in both gels. Finally, from day 7 to day 10, LS174T showed a continuous significant increase of activity in both gels, while HT-29 manifested a significant increase as well, but only in alginate.

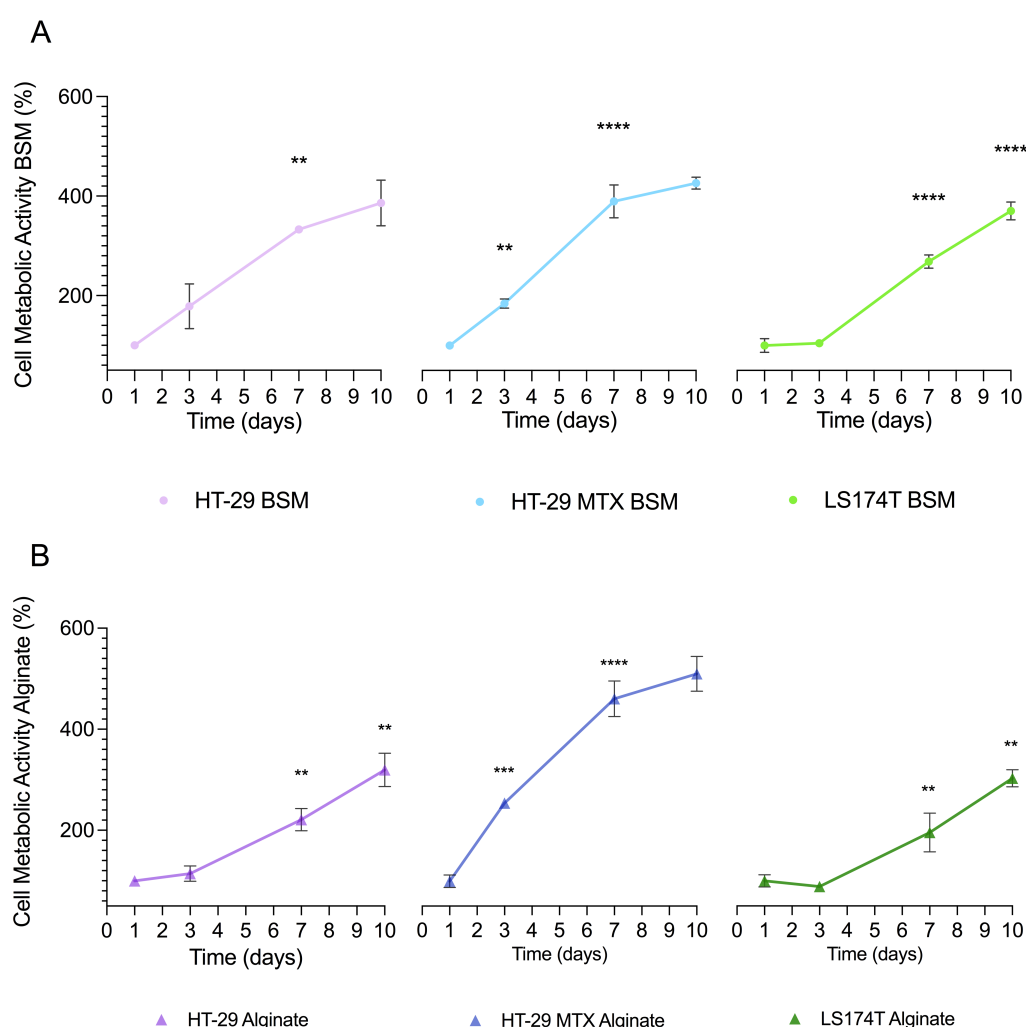


Figure 3.5 The metabolic activity of HT-29, HT-29 MTX and LS174T cells in BSM (A) and alginate (B) assessed by the alamar blue assay. For every condition, the data is normalized to the metabolic activity measurements of day 1. The statistical designation above each time point is a comparison to the previous time point of the same data set. The error bars designate the standard deviation as obtained from measurements of  $n = 3$  independent experiments. Statistical significance was obtained by one-way ANOVA test by Prism 9.0. \*, \*\*, \*\*\*, and \*\*\*\* indicate  $p$  values of  $<0.0332$ ,  $0.0021$ ,  $0.0002$ , and  $0.0001$ , respectively.

The biochemical oxidation-reduction reactions are ubiquitous and indispensable for balance in the body. The health state of cells within a population can be determined by a cell viability assay. In this work, the alamar blue assay was performed to measure metabolic activity, in which the reducing environment of living/viable cells not only changes the color of the reagent from blue to pink or purple, but also provides it with high fluorescence.

Cell proliferation usually elucidate alterations in the number of cells in a cell population. Cell metabolism contributes to the reducing environment of cells within the cytosol, which causes alamar blue reagent to be reduced and change its color, with the advantage of being soluble and non-toxic. Ultimately, this colorimetric REDOX indicator is a measurement tool of the reduction of the intracellular environment. It is important to note that although the detection of the metabolic activity can be a reflection of cell proliferation, the fluorescence signal can be affected by changes in cell number and cell metabolism as well. To investigate the cell viability in gels at this point of the project, but also to test cytotoxicity of anti-cancer drugs in different conditions posteriorly, it was an appropriate method to use given the number of experimental and biological repeats involved in every assay and the practicality of instruments required. Nonetheless, there are other methods to assess cell proliferation, such as utilizing Ki-67 antibody against the Ki67 protein to detect it in the proliferative stages of the cell cycle (S-, G2- and M-) in human cells. Another method would be detecting the ATP content in cells, since it is strictly controlled. Moreover, dead or imminent dead cells contain nearly no ATP and there is a linear relation between the concentration of ATP in cells and the number of cells. Lastly, DNA synthesis assays could be used as well, for its accuracy and reliability of incorporation of radiolabels in the newly proliferated DNA. Regardless, the said methods would not be as functional as the alamar blue assay, for they are more time-consuming, economically demanding and might require a more complex equipment [102]–[104]. Although alamar blue assay is not a direct method of cell proliferation, the rapid increase in metabolic activity and a higher metabolic activity reached in both gels suggest that HT-29 MTX cells seem to proliferate at a faster rate than other cells, and slow down between days 7 and 10. Instead, LS174T cells seemed to be slower to proliferate initially, though from day 3 forward the cell proliferation was steady. Following this reasoning, HT-29 and LS174T cells multiplied slower in the alginate gel than BSM, while HT-29 MTX demonstrated a similar behavior approximately, independently of the hydrogel used in encapsulation. An increase in metabolic activity was achieved in both gels (Figure 3.5), even though there were differences between cell lines and type of gel. HT-29 had a 4- and 3- fold increase in metabolic activity in BSM and Alginate; HT-29 MTX had a 4- and 5-fold increase in BSM and alginate and LS174T had a 4- and 3-fold increase in BSM and alginate. Overall, it was proved that the CRC cell lines selected for this work can live in BSM and alginate. A further study for a longer period of time could be necessary to broaden the perspective of the metabolic activity trend.

Substantially, the fact that cell metabolic activity was increasing and spheroids were growing hints that there was proliferation involved. Hydrogel crosslinking and functionalization chemistry were compatible with living cells. Therefore, muc-gel and alginate can be considered appropriate platforms for cell encapsulation.

### 3.3 5-FU efficacy is affected by the presence of BSM and alginate

The anti-cancer drug 5-FU was administered to HT-29, HT-29 MTX and LS174T cells. Here, all cell lines were challenged according to the 2D model: seeded with a layer of gel covering the cell layer (2D), revealing a barrier effect of the gels against 5-FU. Images of the cytotoxic effect of 5-FU can be found in Figure 5.2.

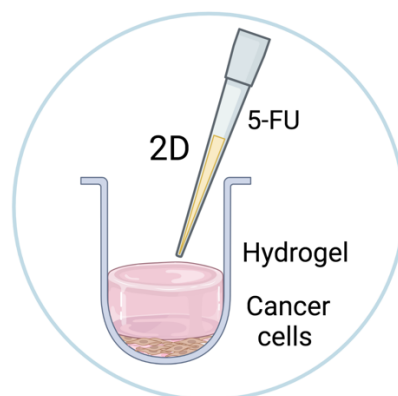


Figure 3.6 Visual representation of the 2D model used in the drug resistance assay. In each well of a 96-well plate there were two layers: a bottom layer with seeded CRC cells and a top layer of hydrogel covering the cells. 5-FU was added at different concentrations for 24 h and a cell metabolic activity assay was carried out.

#### 3.3.1 BSM acts as a physical barrier against 5-FU

Cells covered by BSM showed an increased cell viability when compared with the no gel condition (Figure 3.7). In this context, an increased cell viability can be associated with a greater resistance to the drug. This was more prominent in the case of LS174T, in which at every concentration of 5-FU the difference between the absence of gel on top and BSM was statistically significant at every 5-FU concentration (Figure 3.7). HT-29 with BSM on top at 0.5 mM of 5-FU was the only condition revealing a slightly weaker performance of BSM as a barrier against the anti-cancer drug. The last-mentioned condition and all the remaining others did not exhibit a significant difference, if one only compares no gel with BSM conditions. However, if the emphasis is laid on each data set individually (Figure 3.8), as the concentration of 5-FU increased the trend of BSM was approximately constant, differing from the decrease observed in the absence of gel. The data referring to HT-29 MTX BSM was widely distributed for each concentration, so another set of experimental repeats would be helpful to form a robust hypothesis regarding the barrier effect of BSM against 5-FU. Still, there was a significant decrease of the mean metabolic activity within the no gel condition going from  $81.2 \pm 5.47\%$  at 0.5 mM to  $58.2 \pm 2.48\%$  at 50.0 mM of 5-FU, and a non-significant change when it came to HT-29 MTX BSM going from  $83.0 \pm 15.5\%$  at 0.5 mM to  $74.9 \pm 12.7\%$  at 50.0 mM. Equivalent observations can be made as to HT-29. Despite the fact that the differences between no gel and BSM were not enough to be considered significant, it seems as if BSM could protect cells from the anti-cancer drug. As the concentration of 5-FU increased, the mean cell metabolic activity was generally maintained with non-significant changes ( $68.6 \pm 2.55\%$  at 0.5 mM,  $70.9 \pm 4.15\%$  at 5 mM and  $76.3 \pm 8.66\%$  at 50 mM), whereas with no gel covering the cells it went

from  $82.3 \pm 10.4\%$  at 0.5 mM to  $56.7 \pm 7.52\%$  at 50 mM. As previously mentioned, LS174T cells indicated more evidently the barrier effect of BSM. In fact, without gel the mean cell metabolic activity was drastically reduced to  $68.9 \pm 6.08\%$  at 0.5 mM, whilst its muc-gel covered counterpart was able to keep  $93.0 \pm 2.95\%$  of the cell population viable. For 5.0 and 50.0 mM of 5-FU the discrepancy was  $64.2 \pm 2.23\%$  and  $45.9 \pm 8.81\%$  without gel to  $90.5 \pm 1.58\%$  and  $84.2 \pm 1.96\%$  with muc-gel, respectively.

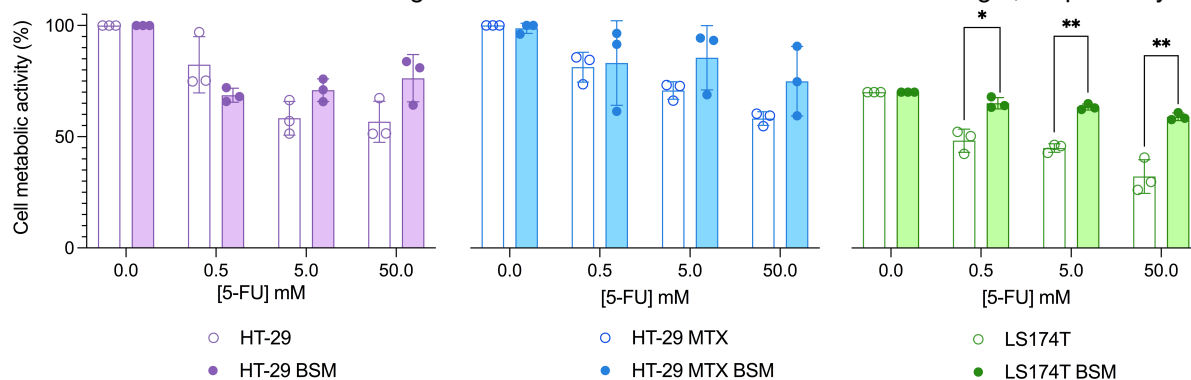


Figure 3.7 Cell metabolic activity of HT-29, HT-29 MTX and LS174T either without hydrogel on the top layer or with BSM and a subsequent treatment with the anti-cancer drug 5-FU at different concentrations (0.0 mM, 0.5 mM, 5.0 mM and 50.0 mM). The error bars denote the standard deviation as obtained from  $n = 3$  independent repeats, each repeat containing triplicates per concentration of 5-FU in question. For every condition, the data was normalized to the metabolic activity corresponding to 0.0 mM. Statistical significance was obtained by one-way ANOVA test by Prism 9.0. \*, \*\*, \*\*\*, and \*\*\*\* indicate  $p$  values of  $<0.0332$ ,  $0.0021$ ,  $0.0002$ , and  $0.0001$ , respectively. For LS174T vs L174T BSM,  $p$  values are  $0.0154$ ,  $0.0013$  and  $0.0021$  for 0.5, 5.0 and 50.0 mM of 5-FU, respectively.

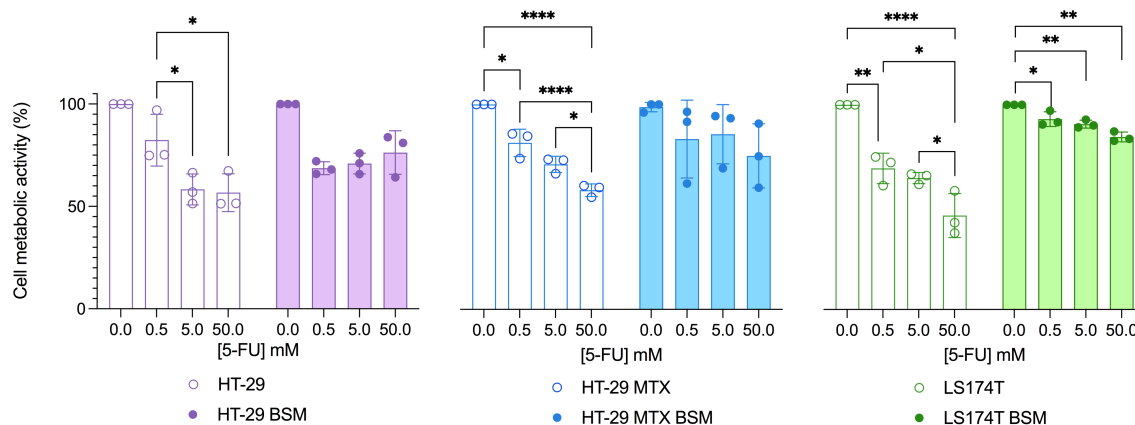


Figure 3.8 Reorganization of data in Figure 3.7 to observe the behavior of no gel and BSM individually. The error bars denote the standard deviation as obtained from  $n = 3$  independent repeats, each repeat containing triplicates per concentration of 5-FU in question. For every condition, the data was normalized to the metabolic activity corresponding to 0.0 mM. Statistical significance was obtained by one-way ANOVA test by Prism 9.0. \*, \*\*, \*\*\*, and \*\*\*\* indicate  $p$  values of  $<0.0332$ ,  $0.0021$ ,  $0.0002$ , and  $0.0001$ , respectively.

### 3.3.2 BSM might provide a stronger barrier effect than alginate

Without exception, all cells with BSM on top showed a higher metabolic activity than cells with alginate at every concentration of 5-FU tested here (Figure 3.9). This disparity between BSM and alginate was specifically significant with LS174T at 5.0 and 50.0 mM of 5-FU:  $90.5 \pm 1.58\%$  in BSM and  $71.9 \pm 6.22\%$  in alginate and  $84.2 \pm 1.96\%$  and  $73.6 \pm 6.03\%$ , respectively (Figure 3.10). Moreover, the performance of cells without gel showed a consistent trend of higher cell viability than cells with alginate, except when 50.0 mM were added to HT-29 MTX and LS174T (Figure 5.3).

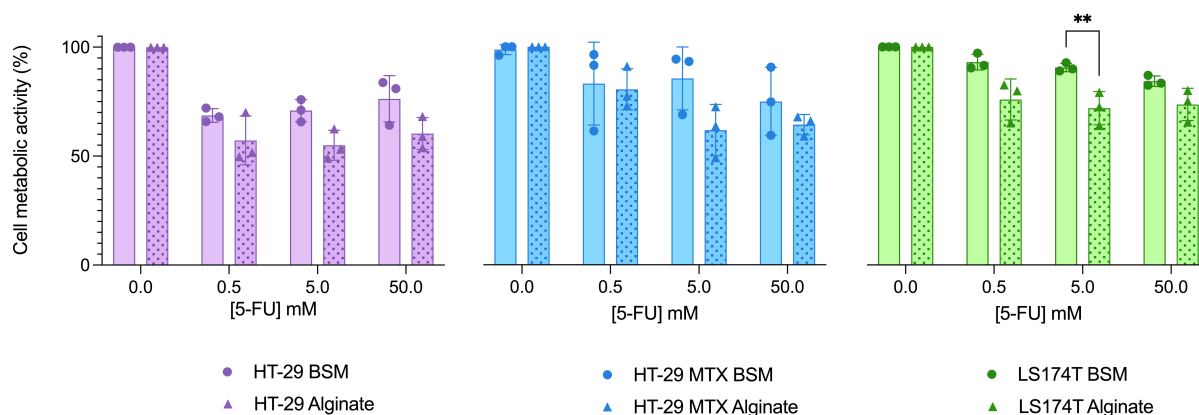


Figure 3.9 Cell metabolic activity of HT-29, HT-29 MTX and LS174T either with hydrogel on the top layer or with BSM, and a subsequent treatment with the anti-cancer drug 5-FU at different concentrations (0.0 mM, 0.5 mM, 5.0 mM and 50.0 mM). The error bars denote the standard deviation as obtained from  $n=3$  independent repeats, each repeat containing triplicates per concentration of 5-FU in question. For every condition, the data was normalized to the metabolic activity corresponding to 0.0 mM. Statistical significance was obtained by one-way ANOVA test by Prism 9.0. \*, \*\*, \*\*\*, and \*\*\*\* indicate  $p$  values of  $<0.0332$ ,  $0.0021$ ,  $0.0002$ , and  $0.0001$ , respectively. At 5.0 mM of 5-FU in LS174T BSM vs LS174T alginate, the  $p$  value is 0.0075.

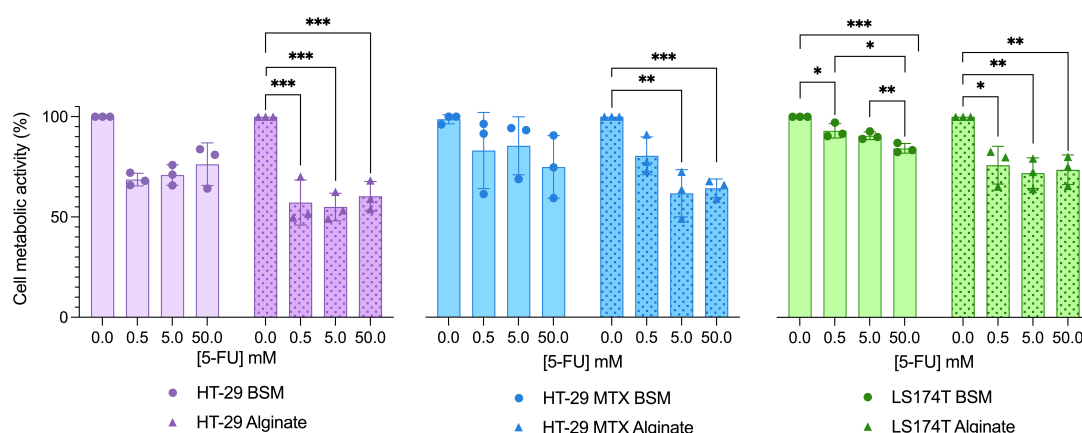


Figure 3.10 Reorganization of data in Figure 3.9 to observe the behaviors of BSM and alginate individually. The error bars denote the standard deviation as obtained from  $n = 3$  independent repeats, each repeat containing triplicates per concentration of 5-FU in question. For every condition, the data was normalized to the metabolic activity corresponding to 0.0 mM. Statistical significance was obtained by one-way ANOVA test by Prism 9.0. \*, \*\*, \*\*\*, and \*\*\*\* indicate  $p$  values of  $<0.0332$ ,  $0.0021$ ,  $0.0002$ , and  $0.0001$ , respectively.



One way to examine carefully the differences in 5-FU cytotoxicity observed between crosslinked gels would be to compare the diffusion. Often, the precise prediction of drug release kinetics from gels also depends on the accurate knowledge of the diffusion coefficient of the solute. Anyhow, biopolymer-based hydrogels such as mucus or the extracellular matrix act as protective barriers against pathogens and toxic agents. As a matter of fact, the mechanisms capable of elucidating the selective permeability of this barrier are not fully understood yet, and hamper the total leverage of mucins in the biotechnology and biomedical fields [105]. While in human tissues *in vivo*, cells are embedded in a physiological extracellular matrix (ECM), in this model the cells are embedded in a ECM-like matrix. Thus, the more appropriate the stiffness and composition, the more successful the model is to mimic diseased micro-environments. ECM is known to have hyaluronan (HA), structural proteins (e.g. collagen) and adhesion peptides/proteins in its composition [106]. As mentioned before, BSM has a complex chemistry with both hydrophobic and hydrophilic domains and a variety of different interactions, making it prone to hamper the diffusion of drugs. For instance, mucin O-glycosylation limits the success of 5-FU by decreasing its uptake against the growth of human pancreatic cancer cells [107]. Chemical differences between BSM and alginate could explain the reason why the latter might have provided a less strong barrier. In addition, an interesting analysis would be to conduct a scanning electron microscopy (SEM) with a focus on the porosity of BSM and alginate, as an attempt to relate the mechanical properties of the gel's network to the performance of 5-FU against cancer cells.

### 3.4 Encapsulation of CRC cells in BSM hints at a potential biological barrier

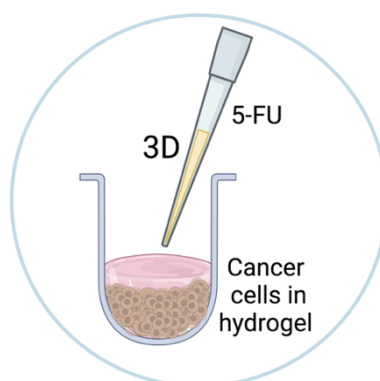


Figure 3.11 Visual representation of the 3D model used in the drug resistance assay. In each well of a 96-well plate CRC cells were encapsulated in BSM or alginate. 5-FU was added at different concentrations for 24 h and a cell metabolic activity assay was carried out.

Cancer cells cultured in a two-dimensional (2D) environment supply an elementary *in vitro* model to screen chemical compounds for drug discovery, but can not afford to have structural, biological and functional similarities from those being cultured in a more complex three-dimensional (3D) model. That being the case, there has been an exceptional interest in the development of 3D cultures that better mimic native tumors [108]. Here, HT-29, HT-29 MTX and LS174T cells were encapsulated (3D) either in muc-gel or alg-gel for 6 h or 10 days. Depending on the cell line and type of gel, one could denote potential phenotype alterations. Interestingly, cell metabolic activity concerning the 6 h encapsulation time point corroborated the barrier effect of the hydrogels observed with the 2D model.

Indeed, the transition from a monolayer cell model (2D) to an encapsulation model (3D) allowed to reinforce previously mentioned hypothesis. The 5-FU treatment on the 6 h cell encapsulation condition indicated that 50.0 mM of the drug, which had earlier reduced cell viability to approximately 50% in the 2D model with no gel, was now maintaining cell viability around  $70.0 \pm 3.12\%$  for HT-29,  $76.4 \pm 10.43\%$  for HT-29 MTX, similarly to the range of values obtained for the 2D model with gel. As for LS174T,  $60 \pm 7.56\%$  of the cells were viable at 50.0 mM of 5-FU. 10 days after encapsulation in BSM, HT-29 showed insignificant decreases in cell viability, whereas HT-29 MTX suffered a slight increase both at 5.0 mM ( $76.0 \pm 9.15$  to  $86.2 \pm 7.33\%$ ) and 50.0 mM ( $76.4 \pm 10.4$  to  $77.9 \pm 10.4\%$ ) of 5-FU. LS174T revealed the most noticeable change, going from  $70.2 \pm 6.39\%$  to  $87.6 \pm 5.67\%$  at 5.0 mM and from  $59.6 \pm 7.56\%$  to  $76.2 \pm 5.20\%$  at 50.0 mM). Again, alginate showed consistently lower values of cell viability when compared to BSM under the same conditions. The most peculiar observation was the decrease in cell viability of LS174T after 10 days of encapsulation, although there were no significant increases or decreases if 6 h and 10 days encapsulation are statistically compared.

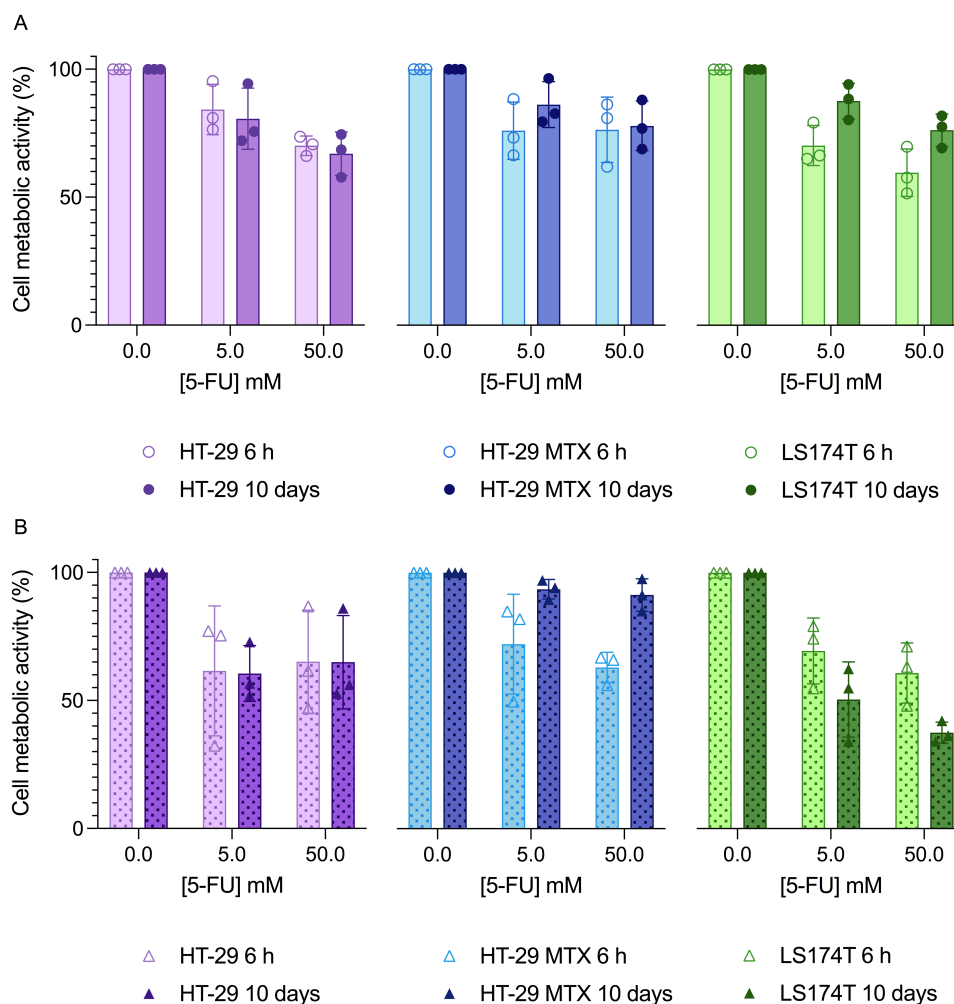


Figure 3.12 Cell metabolic activity of HT-29, HT-29 MTX and LS174T following encapsulation in either BSM (A) or alginate (B) and a subsequent treatment with the anti-cancer drug 5-FU at different concentrations (0.0 mM, 5.0 mM and 50.0 mM). The error bars denote the standard deviation as obtained from  $n=3$  independent repeats, each repeat containing triplicates per concentration of 5-FU. For every condition, the data was normalized to the metabolic activity corresponding to 0.0 mM.

Nonetheless, it is worth to highlight the results of HT-29 MTX in BSM and alginate ( $72.1 \pm 15.9\%$  to  $93.5 \pm 3.01$  at 5.0 mM and  $62.9 \pm 4.85\%$  to  $91.3 \pm 5.16\%$  at 50.0 mM) and LS174T in BSM, denoting an increase that could be of interest.

It is important to clarify that in the 2D model, the cells covered with gel were incubated with 5-FU for 24 h, whereas in the 3D model the cells were incubated for 6 h. With the encapsulation of cells in gel, the aim was to compare a short- and long- term encapsulations and investigate if there were significant changes in cell metabolic activity caused by a longer interaction with BSM and alginate (e.g. phenotypic alterations regarding development of drug resistance). For that, the short-term encapsulation time point was defined as the shortest possible to carry out the experiment within one day of work.

The work of others has suggested that there are two distinct mechanisms for the start of drug resistance in cancer cells: (1) cell phenotypes providing resistance to chemotherapy occur in the tumor prior to treatment and are designated for during the treatment, and (2) cells are induced to develop an acquired resistance as a consequence of treatment [109].

CRC cells manifest resistance in response to anticancer drugs through multiple mechanisms. Some studies have suggested that inhibition of 5-FU-induced cell death and consequent drug resistance is achieved through thymidylate synthase (TS). When the aforesaid enzyme is inhibited by a major 5-FU metabolite (FdUMP), the deoxynucleotide pool necessary for DNA replication is destroyed. Then, 5-FU incorporates its metabolites into RNA and DNA and employs its anti-cancer effects. On the other hand, various studies have proven that the high expression of TS is connected with CRC resistance to 5-FU and intriguingly, the administration of 5-FU itself could augment the expression of that key-enzyme [110]–[112]. 5-FU-resistant CRC cells actually increase TS expression and use a part of this protein to trap FdUMP [113]. With the steady binding of TS to FdUMP, TS is not able to bind to its own mRNA and recovers its enzyme activity. Hence, the drug resistance effect showed when TS mRNA levels were found to be increased. Acquired resistance is related to TS gene (*TYMS*) amplification and mutations [114], which have not developed in these circumstances, since 5-FU was not administered. Perhaps, the results reflect a cell phenotype development occurring prior to treatment.

Considering the changes in cell viability in BSM, it is appealing to pursue additional studies for longer periods of time and take in account the just mentioned mechanism of action of 5-FU by targeting certain genes of resistance. Besides, optimizing the encapsulation method, to attenuate a few limitations encountered in this study and make more assertive conclusions about cell behavior in BSM. Predominantly, the main difficulty was mass producing homogeneously sized spheroids, practical spheroids maintenance for long-term studies, and simple biochemical analysis of drug responses of cells. An alternative would be applying the findings within the Cruzier lab in collaboration with other groups, who recently demonstrated the applicability of negative pressure driven droplet microfluidics and the muc-gel platform as an appropriate micro-encapsulation method, but also as a suitable material for cell culture [68].

### 3.5 MDR and CSCs could be behind the drug resistance of CRC cells in BSM

As mentioned before, the mechanisms by which cells demonstrate resistance against certain drugs are countless, one of them being related to membrane drug transporters. Multi-drug resistance (MDR) can be a result of the membrane transporter expelling drugs to the outside of the cell and perpetuating the viability of tumor cells. Multi-drug resistance protein 1 (MDR-1) is in fact a representative ATP binding cassette (ABC) transporter with a relevant role in CRC resistance to therapy [114].

As hypothesized by Nishida et. al [115], resistance to drugs such as 5-FU could be due to MDR by virtue of increases in the expression and activities of some membrane drug transporters. Moreover, cancer stem cells (CSCs) make up approximately 5% of total tumor cells, having the ability to self-renew, differentiate, participate in tumor initiation and maintenance, metastasis and proliferation. This type of cells has been recognized in diverse cancer types, including colorectal cancer. The mechanism of action of 5-FU triggers the occurrence of reactive oxygen species (ROS) responsible for cancer cell death due to oxidative damage. Still, CSCs can deviate from ROS with an adaptive response that invalidates the action of 5-FU [114], [116]. As unraveled by innumerable studies, CD44 is considered a CSC marker and regulator of many aspects of cancer progression [117], [118].

For the reasons mentioned above, it was considered interesting and appropriate to assess the expression of markers MDR-1 and CD44 in all three types of CRC cells (Figure 3.14). Prior to staining, the cells were exposed to muc- and alg- gels for 6 h and 10 days, similarly to the apparatus presented for the 2D model (Figure 2.4). The fluorescence microscopy images can be found in Figure 5.4 and Figure 5.5.

The results suggest that MDR-1 was found to be significantly higher expressed in HT-29 and LS174T, when comparing 6 h and 10 days of exposure to BSM. On the other hand, no differences were seen in these conditions concerning CD44. After all, and in agreement to a previously denoted 5-FU resistance, MDR might be involved in this drug resistance phenomenon. For HT-29 and HT-29 MTX in alginate gel, there was a significant increase and decrease, respectively, in expression of MDR-1. For HT-29 and HT-29 MTX, there was a significant decrease and increase, respectively, in CD44 expression.

**LS174T**

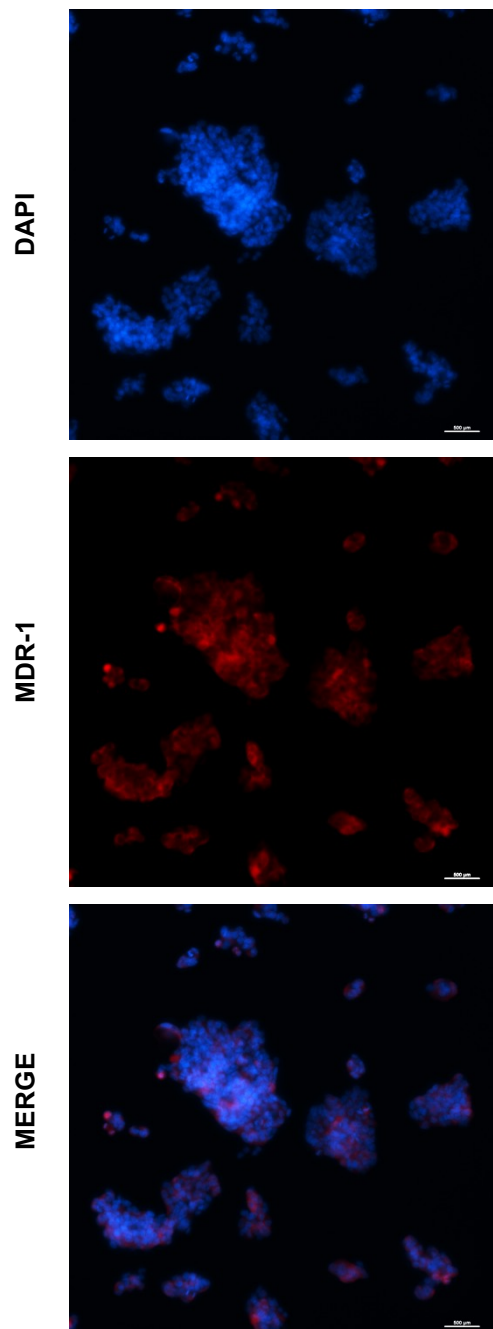


Figure 3.13 Fluorescence microscopy images of MDR-1 expression in LS174T cells. CD44 is not shown here, but incubations with MDR-1 (Excitation/Emission of 590/617 nm) and CD44 (Excitation/Emission of 495/519 nm) antibodies result in membrane staining. Scale bar = 500  $\mu$ m.

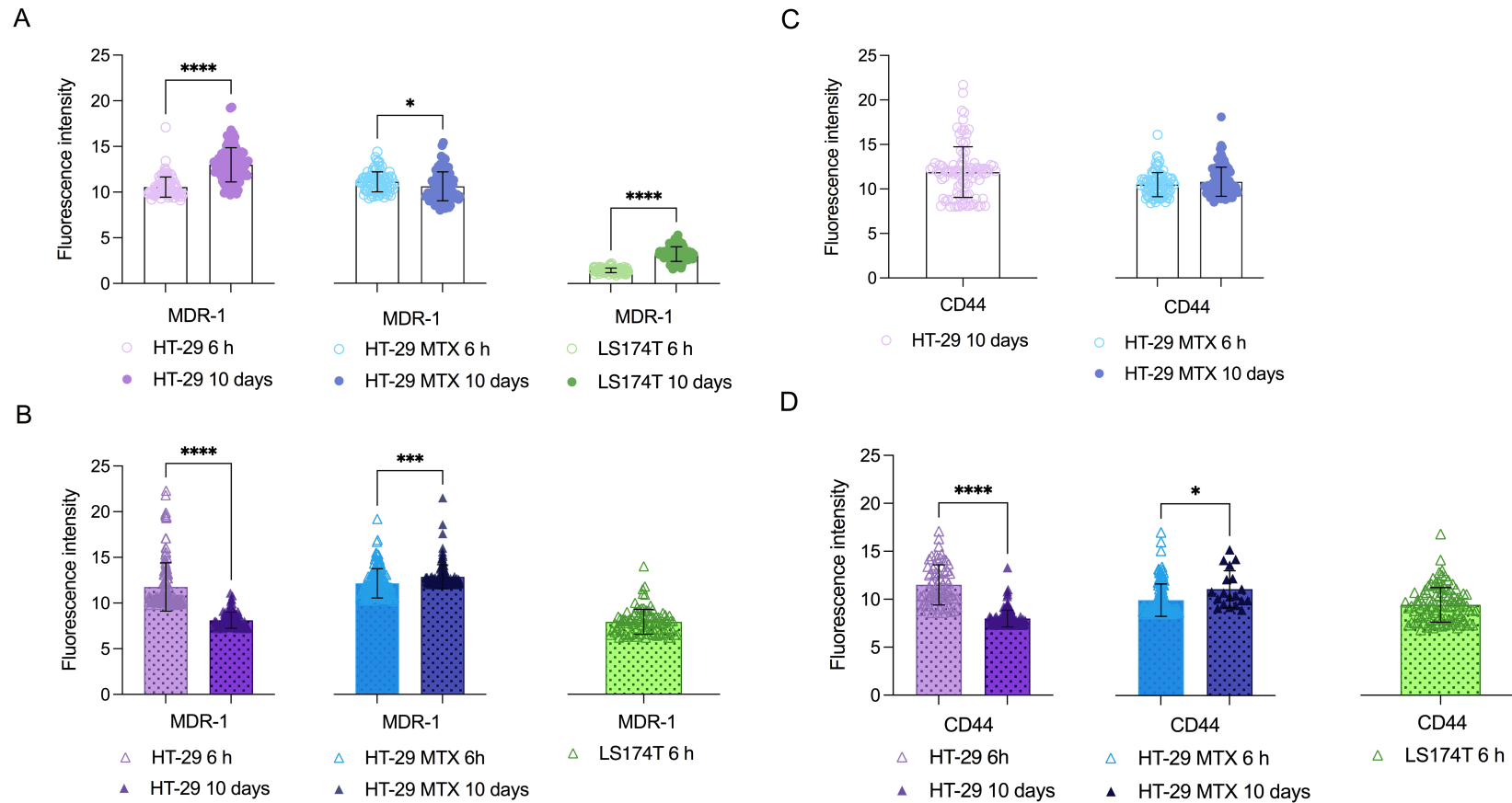


Figure 3.14 Mean fluorescence intensity quantification of MDR-1 in cells exposed to muc-gel (A) and alg-gel (B) for 6 h or 10 days. Quantification of CD44 in cells exposed to muc-gel (C) or alg-gel (D) for either 6 h or 10 days. The error bars denote the standard deviation as obtained from  $n = 3$  images per condition using Cell Profiler software. Statistical significance was obtained by one-way ANOVA test by Prism 9.0. \*, \*\*, \*\*\*, and \*\*\*\* indicate  $p$  values of  $<0.0332$ ,  $0.0021$ ,  $0.0002$ , and  $0.0001$ , respectively. LS174T 10 days, HT-29 6 h and LS174T 10 days conditions are not plotted, due to technical difficulties with the method used. Each mean intensity value corresponds to one object (spheroid).

In this case, a treatment with 5-FU was not implemented. Thus, one can assume an innate resistance to 5-FU from the cells used throughout the project. However, to confirm with certainty that an adaptive resistance is developed it would be more rigorous to administrate 5-FU to the cells prior to initiating the immunofluorescence procedure. Additionally, another method of staining (e.g. immunohistochemistry) could be implemented to allow staining of cancer spheroids, instead of monolayers of cells for more accurate and predictive results, always with the *in vivo* situation in consideration.

## CONCLUSION

Although numerous treatments, such as chemotherapy, targeted therapy, and immunotherapy, are used in clinical practice, the occurrence of drug resistance is the most crucial component in the faulty prognosis of CRC. Tumor cells can shield themselves from the effects of chemotherapy by altering drug metabolism, drug transport, drug targets, and cell death pathways. It is extremely valuable to pursue the comprehension of CRC, specifically mucinous carcinomas, to provide patients with personalized treatments.

Mucins have been the starting point for many exciting projects in the Crouzier group. In this project, some steps were taken to leverage mucin's properties to recreate the *in vivo* microenvironment of mucinous carcinomas *in vitro* while comparing mucin's performance as an encapsulation material with a reference material- alginate. Culture of cancer cells as tumor spheroids is a frequent strategy in cancer research. Spheroids are similar to solid tumors in terms of strong cell-cell connections, cell-matrix interactions, oxygen and nutrition gradients caused by diffusion limitations leading in both proliferative and quiescent cells, hypoxia, and drug delivery challenges.

CRC spheroids grew and proliferated in the muc-gel 3D model, as shown by diameter increases and metabolic activity assays. The challenge of CRC cells both in a monolayer (2D) and encapsulation (3D) cultures pointed in the same direction. The former provided useful information about the physical barrier of mucins towards the anti-cancer drug- perhaps even a stronger barrier than alginate, although more studies are needed to affirm it assertively. The latter encouraged such observations and together with MDR-1 and CD44 expression hinted a potential biological barrier associated with mucin chemistry. These findings are valuable to pursue and improve the application of mucins as an encapsulation material for mucinous cancer cells and narrow the gap of accurate *in vitro* models in cancer research.



## FUTURE WORK

Some adaptations to the existent experiments were suspended, due to lack of time or logistical constraints. Indeed, there were interesting results coming from this work, encouraging the optimization of different techniques. Integrating spheroids into traditional drug discovery has proven to be problematic, due to the difficulties of mass producing identical sized spheroids, practical spheroids maintenance for long-term investigations, and simple biochemical analysis of drug reactions of cells.

First of all, the encapsulation method could be changed in the future to a more automated process, capable of generating similar sized spheroids and facilitating its manipulation, i.e. changing medium, performing viability and drug resistance assays. This could diminish possible inconsistencies when building a hypothesis based on cell viability. With the current method and as seen in previous images, the spheroids are cultured in great proximity to each other from an early stage, possibly promoting cell-cell interactions and inhibiting growth. Additionally, the layout of spheroids was different. Some spheroids were in a higher plan than others, which probably causes variability of O<sub>2</sub> and nutrients access and, consequently, variability of cell metabolic activity. For that matter, the access of drugs might be affected, too. Spheroids closer to the top part of the wells might benefit from a weaker barrier effect when challenged with 5-FU and explain the changes in cell behavior. A break-through would be to include a RNA-seq assay, to characterize the profile of cells and the effect of mucin encapsulation at gene levels. For example, studying the expression of genes of resistance looking closely at the Siglec receptors family. As stated before, BSM can interact with cells through its terminal sugars, which subsequently can bind to cell membrane receptors (e.g. Siglecs). This ligand binding can impact cell signalling, specifically the anti-tumor immune response.

A simple alteration to excute would be to extend the period (days) measuring cell viability and spheroid diameter in the hydrogels, to investigate further the trend of these two parameters, i.e. if it would keep increasing at a steady rate. Another useful addition would be to implement rheology analysis with the alg-gel as well. Here, the muc-gel was analyzed but the mechanical properties of alg-gel were deduced from a thorough study of this gel [55]. The protocol used for chemical synthesis of alg-gel here was also adapted from the said study. Out of curiosity, it would be interesting to perform SEM with both gels to conclude about its porosity and find potential reasons for differences in the drug uptake in BSM and alginate.

Finally, because of logistical difficulties, it was not possible to perform histology staining, which would have been a more rigorous method. That is because it would allow to culture cells in 3D, whereas in the circumstances at the time, the culture had to be carried out in 2D with removal of the gels prior to staining. Otherwise, the antibody would not penetrate the gel layer on top.

## REFERENCES

- [1] G. Petrou and T. Crouzier, “Mucins as multifunctional building blocks of biomaterials,” *Biomater Sci*, vol. 6, no. 9, pp. 2282–2297, Aug. 2018, doi: 10.1039/C8BM00471D.
- [2] M. Uchino and K. Tsubota, “Tear Film Overview,” *Encyclopedia of the Eye*, pp. 263–268, Jan. 2010, doi: 10.1016/B978-0-12-374203-2.00047-6.
- [3] M. D. Walsh *et al.*, “Expression of MUC2, MUC5AC, MUC5B, and MUC6 mucins in colorectal cancers and their association with the CpG island methylator phenotype,” *Modern Pathology*, vol. 26, no. 12, pp. 1642–1656, Dec. 2013, doi: 10.1038/modpathol.2013.101.
- [4] J. Leal, H. D. C. Smyth, and D. Ghosh, “Physicochemical properties of mucus and their impact on transmucosal drug delivery,” *Int J Pharm*, vol. 532, no. 1, p. 555, Oct. 2017, doi: 10.1016/J.IJP.2017.09.018.
- [5] C. L. Hattrup and S. J. Gendler, “Structure and function of the cell surface (tethered) mucins,” *Annual Review of Physiology*, vol. 70, pp. 431–457, 2008. doi: 10.1146/annurev.physiol.70.113006.100659.
- [6] S. Bafna, S. Kaur, and S. K. Batra, “Membrane-bound mucins: the mechanistic basis for alterations in the growth and survival of cancer cells,” *Oncogene 2010 29:20*, vol. 29, no. 20, pp. 2893–2904, Mar. 2010, doi: 10.1038/onc.2010.87.
- [7] M. Tan and D. Yu, “Molecular Mechanisms of ErbB2-Mediated Breast Cancer Chemoresistance,” 2013, Accessed: Jan. 25, 2022. [Online]. Available: <https://www.ncbi.nlm.nih.gov/books/NBK6194/>
- [8] R. Bansil and B. S. Turner, “The biology of mucus: Composition, synthesis and organization ☆,” 2017, doi: 10.1016/j.addr.2017.09.023.
- [9] P. Verdugo, “Mucin exocytosis,” *Am Rev Respir Dis*, vol. 144, no. 3 Pt 2, 1991, doi: 10.1164/AJRCCM/144.3\_PT\_2.S33.
- [10] F. Al-Saedi, A. A. Mohammed, and B. T. Al-Sudani, “Immunocytochemistry of in vitro produced mucin from ht29mtx cell line,” *Indian Journal of Forensic Medicine and Toxicology*, vol. 14, no. 4, pp. 2009–2015, Oct. 2020, doi: 10.37506/IJFMT.V14I4.11842.
- [11] C. Reily, T. J. Stewart, M. B. Renfrow, and J. Novak, “Glycosylation in health and disease”, doi: 10.1038/s41581-019-0129-4.

- [12] T. H. T. Christlet and K. Veluraja, "Database Analysis of O-Glycosylation Sites in Proteins," *Biophys J*, vol. 80, no. 2, pp. 952–960, Feb. 2001, doi: 10.1016/S0006-3495(01)76074-2.
- [13] H. Yan *et al.*, "Immune-Informed Mucin Hydrogels Evade Fibrotic Foreign Body Response In Vivo," *Adv Funct Mater*, vol. 29, no. 46, Nov. 2019, doi: 10.1002/adfm.201902581.
- [14] A. v Kalra and R. B. Campbell, "Mucin impedes cytotoxic effect of 5-FU against growth of human pancreatic cancer cells: overcoming cellular barriers for therapeutic gain," *Br J Cancer*, vol. 97, pp. 910–918, 2007, doi: 10.1038/sj.bjc.6603972.
- [15] G. Javitt *et al.*, "Assembly Mechanism of Mucin and von Willebrand Factor Polymers," *Cell*, vol. 183, no. 3, pp. 717–729.e16, Oct. 2020, doi: 10.1016/J.CELL.2020.09.021.
- [16] G. Javitt and D. Fass, "Helical self-assembly of a mucin segment suggests an evolutionary origin for von Willebrand factor tubules," *Proc Natl Acad Sci U S A*, vol. 119, no. 15, Apr. 2022, doi: 10.1073/PNAS.2116790119/SUPPL\_FILE/PNAS.2116790119.SM02.WMV.
- [17] "The coming of age of glycobiology."
- [18] S. I Gendler and A. P. Spicer, "EPITHELIAL MUCIN GENES," 1995. [Online]. Available: [www.annualreviews.org](http://www.annualreviews.org)
- [19] I. K. Gipson, "0 Human Endocervical Mucins".
- [20] G. Petrou and T. Crouzier, "Biomaterials Science REVIEW Mucins as multifunctional building blocks of biomaterials †," *Cite this: Biomater. Sci*, vol. 6, p. 2282, 2018, doi: 10.1039/c8bm00471d.
- [21] D. J. Thornton and J. K. Sheehan, "From mucins to mucus: toward a more coherent understanding of this essential barrier.," *Proc Am Thorac Soc*, vol. 1, no. 1, pp. 54–61, 2004, doi: 10.1513/PATS.2306016.
- [22] S. K. Linden, P. Sutton, N. G. Karlsson, V. Korolik, and M. A. McGuckin, "Mucins in the mucosal barrier to infection," *Mucosal Immunology 2008 1:3*, vol. 1, no. 3, pp. 183–197, Mar. 2008, doi: 10.1038/mi.2008.5.
- [23] K. Jiang, "Modulating the structure-function relationship of mucin materials." <http://www.diva-portal.org/smash/get/diva2:1634757/FULLTEXT01.pdf> (accessed Jul. 09, 2022).
- [24] M. A. McGuckin, S. K. Lindén, P. Sutton, and T. H. Florin, "Mucin dynamics and enteric pathogens," *Nature Reviews Microbiology 2011 9:4*, vol. 9, no. 4, pp. 265–278, Mar. 2011, doi: 10.1038/nrmicro2538.
- [25] M. E. V. Johansson and G. C. Hansson, "The Mucins," *Encyclopedia of Immunobiology*, vol. 2, pp. 381–388, Jan. 2016, doi: 10.1016/B978-0-12-374279-7.02019-1.
- [26] L. C. Huang, R. L. Redfern, S. Narayanan, R. Y. Reins, and A. M. McDermott, "In Vitro Activity of Human  $\beta$ -Defensin 2 against *Pseudomonas aeruginosa* in the Presence of Tear Fluid," *Antimicrob Agents Chemother*, vol. 51, no. 11, p. 3853, Nov. 2007, doi: 10.1128/AAC.01317-06.
- [27] S. Senapati, S. Das, and S. K. Batra, "Mucin-interacting proteins: from function to therapeutics," *Trends Biochem Sci*, vol. 35, no. 4, pp. 236–245, Apr. 2010, doi: 10.1016/J.TIBS.2009.10.003.
- [28] Y. Yarden and M. X. Sliwkowski, "Untangling the ErbB signalling network," *Nat Rev Mol Cell Biol*, vol. 2, no. 2, pp. 127–137, Feb. 2001, doi: 10.1038/35052073.

- [29] M. Kawakubo *et al.*, “Natural antibiotic function of a human gastric mucin against *Helicobacter pylori* infection,” *Science*, vol. 305, no. 5686, pp. 1003–1006, Aug. 2004, doi: 10.1126/SCIENCE.1099250.
- [30] C. Büll, M. H. den Brok, and G. J. Adema, “Sweet escape: sialic acids in tumor immune evasion,” *Biochim Biophys Acta*, vol. 1846, no. 1, pp. 238–246, 2014, doi: 10.1016/J.BBCAN.2014.07.005.
- [31] P. R. Crocker, J. C. Paulson, and A. Varki, “Siglecs and their roles in the immune system,” *Nat Rev Immunol*, vol. 7, no. 4, pp. 255–266, Apr. 2007, doi: 10.1038/NRI2056.
- [32] K. Jiang *et al.*, “Modulating the Bioactivity of Mucin Hydrogels with Crosslinking Architecture,” *Adv Funct Mater*, vol. 31, no. 10, p. 2008428, Mar. 2021, doi: 10.1002/ADFM.202008428.
- [33] M. E. V. Johansson, M. Phillipson, J. Petersson, A. Velcich, L. Holm, and G. C. Hansson, “The inner of the two Muc2 mucin-dependent mucus layers in colon is devoid of bacteria,” *Proc Natl Acad Sci U S A*, vol. 105, no. 39, pp. 15064–15069, Sep. 2008, doi: 10.1073/PNAS.0803124105/SUPPL\_FILE/0803124105SI.PDF.
- [34] L. Antoni *et al.*, “Human colonic mucus is a reservoir for antimicrobial peptides,” *J Crohns Colitis*, vol. 7, no. 12, pp. e652–e664, Dec. 2013, doi: 10.1016/J.CROHNS.2013.05.006/2/7-12-039.JPEG.
- [35] J. C. Onyiah and S. P. Colgan, “Cytokine responses and epithelial function in the intestinal mucosa,” *Cell Mol Life Sci*, vol. 73, no. 22, p. 4203, Jun. 2016, doi: 10.1007/S00018-016-2289-8.
- [36] X. Song, X. He, X. Li, and Y. Qian, “The roles and functional mechanisms of interleukin-17 family cytokines in mucosal immunity,” *Cellular & Molecular Immunology* 2016 13:4, vol. 13, no. 4, pp. 418–431, Mar. 2016, doi: 10.1038/cmi.2015.105.
- [37] J. H. Klinkspoor, K. S. Mok, B. J. W. van Klinken, G. N. J. Tytgat, S. P. Lee, and A. K. Groen, “Mucin secretion by the human colon cell line LS174T is regulated by bile salts,” *Glycobiology*, vol. 9, no. 1, pp. 13–19, Jan. 1999, doi: 10.1093/GLY-COB/9.1.13.
- [38] H. Dolznig *et al.*, “Modeling colon adenocarcinomas in vitro: A 3D co-culture system induces cancer-relevant pathways upon tumor cell and stromal fibroblast interaction,” *American Journal of Pathology*, vol. 179, no. 1, pp. 487–501, Jul. 2011, doi: 10.1016/j.ajpath.2011.03.015.
- [39] A. Olejniczak, M. Szaryńska, and Z. Kmiec, “In vitro characterization of spheres derived from colorectal cancer cell lines,” *Int J Oncol*, vol. 52, no. 2, pp. 599–612, Feb. 2018, doi: 10.3892/ijo.2017.4206.
- [40] J. Ferez-Vilar and R. L. Hill, “The structure and assembly of secreted mucins,” *J Biol Chem*, vol. 274, no. 45, pp. 31751–31754, Nov. 1999, doi: 10.1074/JBC.274.45.31751.
- [41] M. Scawen and A. Allent, “The Action of Proteolytic Enzymes on the Glycoprotein from Pig Gastric Mucus,” *Biochem. J*, vol. 163, pp. 363–368, 1977.
- [42] S. Takehara, M. Yanagishita, K. A. Podyma-Inoue, and Y. Kawaguchi, “Degradation of MUC7 and MUC5B in Human Saliva,” *PLoS One*, vol. 8, no. 7, p. e69059, Jul. 2013, doi: 10.1371/JOURNAL.PONE.0069059.
- [43] V. J. Schömig, B. T. Käsdorf, C. Scholz, K. Bidmon, O. Liele, and S. Berensmeier, “An optimized purification process for porcine gastric mucin with preservation of its native functional properties,” *RSC Adv*, vol. 6, no. 50, pp. 44932–44943, May 2016, doi: 10.1039/C6RA07424C.

- [44] Y. Matsumoto *et al.*, “Identification of Tn antigen O-GalNAc-expressing glycoproteins in human carcinomas using novel anti-Tn recombinant antibodies,” *Glycobiology*, vol. 30, no. 5, p. 282, May 2020, doi: 10.1093/GLYCOB/CWZ095.
- [45] W. Jiang, D. Gupta, D. Gallagher, S. Davis, and V. P. Bhavanandan, “The central domain of bovine submaxillary mucin consists of over 50 tandem repeats of 329 amino acids,” *Eur J Biochem*, vol. 267, no. 8, pp. 2208–2217, Apr. 2000, doi: 10.1046/J.1432-1327.2000.01225.X.
- [46] L. R. Loureiro *et al.*, “Novel monoclonal antibody L2A5 specifically targeting sialyl-Tn and short glycans terminated by alpha-2–6 sialic acids,” *Scientific Reports 2018 8:1*, vol. 8, no. 1, pp. 1–16, Aug. 2018, doi: 10.1038/s41598-018-30421-w.
- [47] C. v. Duffy, L. David, and T. Crouzier, “Covalently-crosslinked mucin biopolymer hydrogels for sustained drug delivery,” *Acta Biomater*, vol. 20, pp. 51–59, Jul. 2015, doi: 10.1016/j.actbio.2015.03.024.
- [48] X. Zhang and Y. Zhang, “Applications of Azide-Based Bioorthogonal Click Chemistry in Glycobiology,” *Molecules*, vol. 18, no. 6, p. 7145, Jun. 2013, doi: 10.3390/MOLECULES18067145.
- [49] N. K. Devaraj, “The Future of Bioorthogonal Chemistry,” *ACS Cent Sci*, vol. 4, no. 8, pp. 952–959, Aug. 2018, doi: 10.1021/ACSCENTSCI.8B00251/ASSET/IMAGES/LARGE/OC-2018-002518\_0004.JPEG.
- [50] H. Oikawa, “Nature’s Strategy for Catalyzing Diels-Alder Reaction,” *Cell Chem Biol*, vol. 23, no. 4, pp. 429–430, Apr. 2016, doi: 10.1016/J.CHEMBIOL.2016.04.002.
- [51] S. L. Scinto *et al.*, “Bioorthogonal chemistry,” *Nature Reviews Methods Primers 2021 1:1*, vol. 1, no. 1, pp. 1–23, Apr. 2021, doi: 10.1038/s43586-021-00028-z.
- [52] E. M. Sletten and C. R. Bertozzi, “Bioorthogonal chemistry: fishing for selectivity in a sea of functionality,” *Angew Chem Int Ed Engl*, vol. 48, no. 38, pp. 6974–6998, Sep. 2009, doi: 10.1002/ANIE.200900942.
- [53] A. Sarkar, F. Xu, and S. Lee, “Human saliva and model saliva at bulk to adsorbed phases – similarities and differences,” *Adv Colloid Interface Sci*, vol. 273, p. 102034, Nov. 2019, doi: 10.1016/J.CIS.2019.102034.
- [54] J. Su, “Thiol-Mediated Chemoselective Strategies for In Situ Formation of Hydrogels,” *Gels 2018, Vol. 4, Page 72*, vol. 4, no. 3, p. 72, Sep. 2018, doi: 10.3390/GELS4030072.
- [55] R. M. Desai, S. T. Koshy, S. A. Hilderbrand, D. J. Mooney, and N. S. Joshi, “Versatile click alginate hydrogels crosslinked via tetrazine–norbornene chemistry,” *Biomaterials*, vol. 50, no. 1, pp. 30–37, May 2015, doi: 10.1016/J.BIOMATERIALS.2015.01.048.
- [56] G. C. Hansson, “Mucus and mucins in diseases of the intestinal and respiratory tracts,” *J Intern Med*, vol. 285, no. 5, p. 479, May 2019, doi: 10.1111/JOIM.12910.
- [57] H. P. Hauber, S. C. Foley, and Q. Hamid, “Mucin overproduction in chronic inflammatory lung disease,” *Canadian Respiratory Journal : Journal of the Canadian Thoracic Society*, vol. 13, no. 6, p. 327, 2006, doi: 10.1155/2006/901417.
- [58] M. C. Rose and J. A. Voynow, “Respiratory tract mucin genes and mucin glycoproteins in health and disease,” *Physiol Rev*, vol. 86, no. 1, pp. 245–278, Jan. 2006, doi: 10.1152/PHYSREV.00010.2005/ASSET/IMAGES/LARGE/Z9J0010623871006.JPEG.
- [59] R. D. Coakley *et al.*, “Abnormal surface liquid pH regulation by cultured cystic fibrosis bronchial epithelium,” *Proc Natl Acad Sci U S A*, vol. 100, no. 26, pp. 16083–16088, Dec. 2003, doi: 10.1073/pnas.2634339100.

- [60] P. Argüeso and I. K. Gipson, “Epithelial mucins of the ocular surface: structure, biosynthesis and function,” *Exp Eye Res*, vol. 73, no. 3, pp. 281–289, 2001, doi: 10.1006/EXER.2001.1045.
- [61] M. A. Hollingsworth and B. J. Swanson, “Mucins in cancer: protection and control of the cell surface,” *Nat Rev Cancer*, vol. 4, no. 1, pp. 45–60, 2004, doi: 10.1038/NRC1251.
- [62] H. Sung *et al.*, “Global Cancer Statistics 2020: GLOBOCAN Estimates of Incidence and Mortality Worldwide for 36 Cancers in 185 Countries,” *CA Cancer J Clin*, vol. 71, no. 3, pp. 209–249, May 2021, doi: 10.3322/caac.21660.
- [63] L. J. M. Mekenkamp *et al.*, “Mucinous adenocarcinomas: Poor prognosis in metastatic colorectal cancer,” *Eur J Cancer*, vol. 48, no. 4, pp. 501–509, Mar. 2012, doi: 10.1016/j.ejca.2011.12.004.
- [64] N. Hugén, G. Brown, R. Glynne-Jones, J. H. W. de Wilt, and I. D. Nagtegaal, “Advances in the care of patients with mucinous colorectal cancer,” *Nature Reviews Clinical Oncology*, vol. 13, no. 6. Nature Publishing Group, pp. 361–369, Jun. 01, 2016. doi: 10.1038/nrclinonc.2015.140.
- [65] S. Nakamori, D. M. Ota, K. R. Cleary, K. Shirotani, and T. Irimura, “MUC1 Mucin Expression as a Marker of Progression and Metastasis of Human Colorectal Carcinoma,” *Gastroenterology*, vol. 106, pp. 363–361, 1994.
- [66] J. C. Byrd and R. S. Bresalier, “Mucins and mucin binding proteins in colorectal cancer,” Kluwer Academic Publishers, 2004.
- [67] G. Cantero-Recasens *et al.*, “Reversing chemorefraction in colorectal cancer cells by controlling mucin secretion,” *Elife*, vol. 11, Feb. 2022, doi: 10.7554/ELIFE.73926.
- [68] H. Yan *et al.*, “Immune-Modulating Mucin Hydrogel Microdroplets for the Encapsulation of Cell and Microtissue,” *Adv Funct Mater*, vol. 31, no. 42, Oct. 2021, doi: 10.1002/adfm.202105967.
- [69] C. H. M. J. van Elssen *et al.*, “Expression of aberrantly glycosylated Mucin-1 in ovarian cancer,” *Histopathology*, vol. 57, no. 4, pp. 597–606, Oct. 2010, doi: 10.1111/J.1365-2559.2010.03667.X.
- [70] C. R. Boland and G. D. Deshmukh, “The carbohydrate composition of mucin in colonic cancer,” *Gastroenterology*, vol. 98, no. 5 Pt 1, pp. 1170–1177, 1990, doi: 10.1016/0016-5085(90)90330-4.
- [71] N. Zhang, Y. Yin, S.-J. Xu, and W.-S. Chen, “molecules 5-Fluorouracil: Mechanisms of Resistance and Reversal Strategies,” *Molecules*, vol. 13, pp. 1551–1569, 2008, doi: 10.3390/molecules13081551.
- [72] J. Y. Douillard *et al.*, “Irinotecan combined with fluorouracil compared with fluorouracil alone as first-line treatment for metastatic colorectal cancer: a multicentre randomised trial,” *Lancet*, vol. 355, no. 9209, pp. 1041–1047, Mar. 2000, doi: 10.1016/S0140-6736(00)02034-1.
- [73] T. McFall and E. C. Stites, “Identification of RAS mutant biomarkers for EGFR inhibitor sensitivity using a systems biochemical approach,” *Cell Rep*, vol. 37, no. 11, p. 110096, Dec. 2021, doi: 10.1016/j.celrep.2021.110096.
- [74] S. Sigismund, D. Avanzato, L. Lanzetti, and L. Lanzetti, “Emerging functions of the EGFR in cancer,” 2017, doi: 10.1002/1878-0261.12155.
- [75] M. S. Miller and L. D. Miller, “RAS mutations and oncogenesis: Not all RAS mutations are created equally,” *Front Genet*, vol. 2, no. JAN, p. 100, 2012, doi: 10.3389/FGENE.2011.00100/BIBTEX.

- [76] D. K. Simanshu, D. v. Nissley, and F. McCormick, “RAS Proteins and Their Regulators in Human Disease,” *Cell*, vol. 170, no. 1, p. 17, Jun. 2017, doi: 10.1016/J.CELL.2017.06.009.
- [77] T. McFall and E. C. Stites, “Identification of RAS mutant biomarkers for EGFR inhibitor sensitivity using a systems biochemical approach,” *Cell Rep*, vol. 37, no. 11, p. 110096, Dec. 2021, doi: 10.1016/j.celrep.2021.110096.
- [78] S. Pascual-Gil and S. Epelman, “Monocyte-Derived Macrophages: The Missing Link in Organ Transplantation,” *Immunity*, vol. 49, no. 5, pp. 783–785, Nov. 2018, doi: 10.1016/J.IMMUNI.2018.11.005.
- [79] L. Davenport Huyer, S. Pascual-Gil, Y. Wang, S. Mandla, B. Yee, and M. Radisic, “Advanced Strategies for Modulation of the Material–Macrophage Interface,” *Adv Funct Mater*, vol. 30, no. 44, Oct. 2020, doi: 10.1002/ADFM.201909331.
- [80] T. L. Carlson, J. Y. Lock, and R. L. Carrier, “Engineering the Mucus Barrier,” *Annu Rev Biomed Eng*, vol. 20, p. 197, Jun. 2018, doi: 10.1146/ANNUREV-BIOENG-062117-121156.
- [81] M. C. McKelvey, R. Brown, S. Ryan, M. A. Mall, S. Weldon, and C. C. Taggart, “Proteases, Mucus, and Mucosal Immunity in Chronic Lung Disease,” *Int J Mol Sci*, vol. 22, no. 9, May 2021, doi: 10.3390/IJMS22095018.
- [82] A. Curnutt, K. Smith, E. Darrow, and K. B. Walters, “Chemical and Microstructural Characterization of pH and [Ca<sup>2+</sup>] Dependent Sol-Gel Transitions in Mucin Biopolymer,” *Sci Rep*, vol. 10, no. 1, Dec. 2020, doi: 10.1038/S41598-020-65392-4.
- [83] H. M. Yildiz, L. Speciner, C. Ozdemir, D. E. Cohen, and R. L. Carrier, “Food-associated Stimuli Enhance Barrier Properties of Gastrointestinal Mucus,” *Biomaterials*, vol. 54, p. 1, Jun. 2015, doi: 10.1016/J.BIOMATERIALS.2015.02.118.
- [84] K. R. Bhaskar *et al.*, “Profound increase in viscosity and aggregation of pig gastric mucin at low pH,” *Am J Physiol*, vol. 261, no. 5 Pt 1, 1991, doi: 10.1152/AJ-PGI.1991.261.5.G827.
- [85] X. Cao *et al.*, “pH-dependent conformational change of gastric mucin leads to sol-gel transition,” *Biophys J*, vol. 76, no. 3, pp. 1250–1258, 1999, doi: 10.1016/S0006-3495(99)77288-7.
- [86] T. L. Carlson, H. Yildiz, Z. Dar, J. Y. Lock, and R. L. Carrier, “Lipids alter microbial transport through intestinal mucus,” *PLoS One*, vol. 13, no. 12, Dec. 2018, doi: 10.1371/JOURNAL.PONE.0209151.
- [87] F. Guilak, D. M. Cohen, B. T. Estes, J. M. Gimble, W. Liedtke, and C. S. Chen, “Control of stem cell fate by physical interactions with the extracellular matrix,” *Cell Stem Cell*, vol. 5, no. 1, pp. 17–26, Jul. 2009, doi: 10.1016/J.STEM.2009.06.016.
- [88] K. Y. Lee and D. J. Mooney, “Hydrogels for tissue engineering,” *Chem Rev*, vol. 101, no. 7, pp. 1869–1879, Jul. 2001, doi: 10.1021/CR000108X.
- [89] N. F. Huang and S. Li, “Regulation of the matrix microenvironment for stem cell engineering and regenerative medicine,” *Ann Biomed Eng*, vol. 39, no. 4, p. 1201, Apr. 2011, doi: 10.1007/S10439-011-0297-2.
- [90] B. D. Ratner and S. J. Bryant, “Biomaterials: where we have been and where we are going,” *Annu Rev Biomed Eng*, vol. 6, pp. 41–75, 2004, doi: 10.1146/ANNUREV.BIO-ENG.6.040803.140027.
- [91] C. M. Madl and S. C. Heilshorn, “Bioorthogonal Strategies for Engineering Extracellular Matrices,” *Adv Funct Mater*, vol. 28, no. 11, p. 1706046, Mar. 2018, doi: 10.1002/ADFM.201706046.

- [92] E. M. Sletten and C. R. Bertozzi, "From mechanism to mouse: A tale of two bioorthogonal reactions," *Acc Chem Res*, vol. 44, no. 9, pp. 666–676, Sep. 2011, doi: 10.1021/AR200148Z/ASSET/IMAGES/LARGE/AR-2011-00148Z\_0014.JPEG.
- [93] W. R. Algar, P. E. Dawson, and I. L. Medintz, "Chemoselective and bioorthogonal ligation reactions. volume 1 and 2 : concepts and applications", Accessed: Sep. 27, 2022. [Online]. Available: <https://www.wiley.com/en-us/Chemoselective+and+Bioorthogonal+Ligation+Reactions%3A+Concepts+and+Applications-p-9783527334360>
- [94] D. M. Patterson, L. A. Nazarova, and J. A. Prescher, "Finding the right (bioorthogonal) chemistry," *ACS Chemical Biology*, vol. 9, no. 3. American Chemical Society, pp. 592–605, Mar. 21, 2014. doi: 10.1021/cb400828a.
- [95] B. L. Oliveira, Z. Guo, and G. J. L. Bernardes, "Inverse electron demand Diels–Alder reactions in chemical biology," *Chem Soc Rev*, vol. 46, no. 16, pp. 4895–4950, Aug. 2017, doi: 10.1039/C7CS00184C.
- [96] S. Fé Ré Ol, R. Fodil, M. Laurent, B. Louis, D. Isabey, and E. Planus, "Sensitivity of Alveolar Macrophages to Substrate Mechanical and Adhesive Properties", doi: 10.1002/cm.20130.
- [97] A. K. Blakney, M. D. Swartzlander, and S. J. Bryant, "The effects of substrate stiffness on the in vitro activation of macrophages and in vivo host response to poly(ethylene glycol)-based hydrogels," *J Biomed Mater Res A*, vol. 100, no. 6, pp. 1375–1386, Jun. 2012, doi: 10.1002/JBM.A.34104.
- [98] J. A. Flegg and N. Nataraj, "Mathematical Modelling and Avascular Tumour Growth," *Resonance 2019 24:3*, vol. 24, no. 3, pp. 313–325, May 2019, doi: 10.1007/S12045-019-0782-8.
- [99] L. Spoerri, G. Gunasingh, and N. K. Haass, "Fluorescence-Based Quantitative and Spatial Analysis of Tumour Spheroids: A Proposed Tool to Predict Patient-Specific Therapy Response," *Front Digit Health*, vol. 3, May 2021, doi: 10.3389/FDGTH.2021.668390.
- [100] D. I. Wallace and X. Guo, "Properties of tumor spheroid growth exhibited by simple mathematical models," *Front Oncol*, vol. 3 MAR, p. 51, 2013, doi: 10.3389/FONC.2013.00051/BIBTEX.
- [101] A. P. Browning *et al.*, "Quantitative analysis of tumour spheroid structure," vol. 10, 2021, doi: 10.7554/eLife.73020.
- [102] A. Adan, Y. Kiraz, and Y. Baran, "Cell Proliferation and Cytotoxicity Assays," *Curr Pharm Biotechnol*, vol. 17, no. 14, pp. 1213–1221, Aug. 2016, doi: 10.2174/1389201017666160808160513.
- [103] M. J. Stoddart, "Cell viability assays: introduction," *Methods Mol Biol*, vol. 740, pp. 1–6, 2011, doi: 10.1007/978-1-61779-108-6\_1.
- [104] S. N. Rampersad, "Multiple Applications of Alamar Blue as an Indicator of Metabolic Function and Cellular Health in Cell Viability Bioassays," *Sensors (Basel)*, vol. 12, no. 9, p. 12347, Sep. 2012, doi: 10.3390/S120912347.
- [105] M. Quesada-Pérez, J. A. Maroto-Centeno, M. del M. Ramos-Tejada, and A. Martín-Molina, "Universal description of steric hindrance in flexible polymer gels," *Physical Chemistry Chemical Physics*, vol. 23, no. 28, pp. 14997–15002, Jul. 2021, doi: 10.1039/D1CP02113C.
- [106] P. Lu, V. M. Weaver, and Z. Werb, "The extracellular matrix: A dynamic niche in cancer progression," *J Cell Biol*, vol. 196, no. 4, p. 395, Feb. 2012, doi: 10.1083/JCB.201102147.



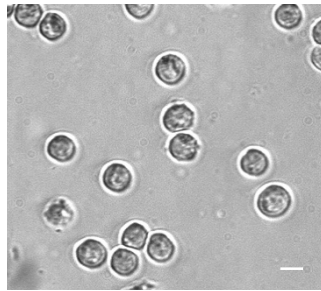
- [107] A. v. Kalra and R. B. Campbell, “Mucin overexpression limits the effectiveness of 5-FU by reducing intracellular drug uptake and antineoplastic drug effects in pancreatic tumours,” *Eur J Cancer*, vol. 45, no. 1, pp. 164–173, Jan. 2009, doi: 10.1016/J.EJCA.2008.10.008.
- [108] P. S. Thakuri, M. Gupta, M. Plaster, and H. Tavana, “Quantitative Size-Based Analysis of Tumor Spheroids and Responses to Therapeutics,” *Assay Drug Dev Technol*, vol. 17, no. 3, pp. 140–149, Apr. 2019, doi: 10.1089/ADT.2018.895.
- [109] N. Kumar, G. M. Cramer, S. A. Z. Dahaj, B. Sundaram, J. P. Celli, and R. v. Kulkarni, “Stochastic modeling of phenotypic switching and chemoresistance in cancer cell populations,” *Scientific Reports 2019 9:1*, vol. 9, no. 1, pp. 1–10, Jul. 2019, doi: 10.1038/s41598-019-46926-x.
- [110] L. Chen, F. Yang, S. Chen, and J. Tai, “Mechanisms on chemotherapy resistance of colorectal cancer stem cells and research progress of reverse transformation: A mini-review,” *Front Med (Lausanne)*, vol. 0, p. 2592, Sep. 2022, doi: 10.3389/FMED.2022.995882.
- [111] K. van der Jeught, H. C. Xu, Y. J. Li, X. bin Lu, and G. Ji, “Drug resistance and new therapies in colorectal cancer,” *World J Gastroenterol*, vol. 24, no. 34, p. 3834, Sep. 2018, doi: 10.3748/WJG.V24.I34.3834.
- [112] Q. Wang, X. Shen, G. Chen, and J. Du, “Drug Resistance in Colorectal Cancer: From Mechanism to Clinic,” 2022, doi: 10.3390/cancers.
- [113] C. Kurasaka, N. Nishizawa, Y. Ogino, and A. Sato, “Trapping of 5-Fluorodeoxyuridine Monophosphate by Thymidylate Synthase Confers Resistance to 5-Fluorouracil,” *ACS Omega*, vol. 7, no. 7, pp. 6046–6052, Feb. 2022, doi: 10.1021/ACSOMEGA.1C06394/ASSET/IMAGES/LARGE/AO1C06394\_0005.JPEG.
- [114] S. Blondy, V. David, M. Verdier, M. Mathonnet, A. Perraud, and N. Christou, “5-Fluorouracil resistance mechanisms in colorectal cancer: From classical pathways to promising processes,” *Cancer Sci*, vol. 111, no. 9, pp. 3142–3154, Sep. 2020, doi: 10.1111/CAS.14532.
- [115] N. Nishida *et al.*, “MicroRNA-10b is a prognostic indicator in colorectal cancer and confers resistance to the chemotherapeutic agent 5-fluorouracil in colorectal cancer cells,” *Ann Surg Oncol*, vol. 19, no. 9, pp. 3065–3071, Sep. 2012, doi: 10.1245/S10434-012-2246-1.
- [116] X. Li, H. Zhao, X. Zhou, and L. Song, “Inhibition of lactate dehydrogenase A by microRNA.34a resensitizes colon cancer cells to 5.fluorouracil,” *Mol Med Rep*, vol. 11, no. 1, pp. 577–582, Jan. 2015, doi: 10.3892/MMR.2014.2726/HTML.
- [117] L. Wang, X. Zuo, K. Xie, and D. Wei, “The Role of CD44 and Cancer Stem Cells,” *Methods Mol Biol*, vol. 1692, pp. 31–42, 2018, doi: 10.1007/978-1-4939-7401-6\_3.
- [118] H. Xu, M. Niu, X. Yuan, K. Wu, and A. Liu, “CD44 as a tumor biomarker and therapeutic target”, doi: 10.1186/s40164-020-00192-0.
- [119] K. A. McClellan, “Mucosal defense of the outer eye,” *Surv Ophthalmol*, vol. 42, no. 3, pp. 233–246, 1997, doi: 10.1016/S0039-6257(97)00090-8.
- [120] “Immunity in the salivary gland | British Society for Immunology.” <https://www.immunology.org/public-information/bitesized-immunology/organs-and-tissues/immunity-in-the-salivary-gland> (accessed Jul. 08, 2022).
- [121] M. C. Rose and J. A. Voynow, “Respiratory tract mucin genes and mucin glycoproteins in health and disease,” *Physiol Rev*, vol. 86, no. 1, pp. 245–278, Jan. 2006, doi: 10.1152/PHYSREV.00010.2005/ASSET/IMAGES/LARGE/Z9J0010623871006.JPEG.

- [122] M. Herath, S. Hosie, J. C. Bornstein, A. E. Franks, and E. L. Hill-Yardin, “The Role of the Gastrointestinal Mucus System in Intestinal Homeostasis: Implications for Neurological Disorders,” *Front Cell Infect Microbiol*, vol. 10, p. 248, May 2020, doi: 10.3389/FCIMB.2020.00248/BIBTEX.
- [123] J. A. Grondin, Y. H. Kwon, P. M. Far, S. Haq, and W. I. Khan, “Mucins in Intestinal Mucosal Defense and Inflammation: Learning From Clinical and Experimental Studies,” *Front Immunol*, vol. 11, p. 2054, Sep. 2020, doi: 10.3389/FIMMU.2020.02054/BIBTEX.
- [124] T. Kurita, “Cervix: Cell Biology,” *Encyclopedia of Reproduction*, pp. 347–352, Jan. 2018, doi: 10.1016/B978-0-12-801238-3.64405-7.
- [125] R. Shogren, T. A. Gerken, and N. Jentoft, “Role of glycosylation on the conformation and chain dimensions of O-linked glycoproteins: light-scattering studies of ovine submaxillary mucin,” *Biochemistry*, vol. 28, no. 13, pp. 5525–5536, Jun. 1989, doi: 10.1021/BI00439A029.
- [126] W. W. Sun *et al.*, “Nanoarchitecture and dynamics of the mouse enteric glycocalyx examined by freeze-etching electron tomography and intravital microscopy,” *Communications Biology* 2020 3:1, vol. 3, no. 1, pp. 1–10, Jan. 2020, doi: 10.1038/s42003-019-0735-5.
- [127] P. Alard *et al.*, “Interactions of Intestinal Bacteria with Components of the Intestinal Mucus,” *Frontiers in Cellular and Infection Microbiology* | [www.frontiersin.org](http://www.frontiersin.org), vol. 7, p. 387, 2017, doi: 10.3389/fcimb.2017.00387.
- [128] “Mucolytics, expectorants, and mucokinetic medications | Request PDF.” [https://www.researchgate.net/publication/6242212\\_Mucolytics\\_expectorants\\_and\\_mucokinetic\\_medications](https://www.researchgate.net/publication/6242212_Mucolytics_expectorants_and_mucokinetic_medications) (accessed Aug. 04, 2022).
- [129] J. S. Suk, S. K. Lai, N. J. Boylan, M. R. Dawson, M. P. Boyle, and J. Hanes, “Rapid transport of muco-inert nanoparticles in cystic fibrosis sputum treated with N-acetyl cysteine,” *Nanomedicine (Lond)*, vol. 6, no. 2, pp. 365–375, Feb. 2011, doi: 10.2217/NNM.10.123.
- [130] M. O. Henke and F. Ratjen, “Mucolytics in cystic fibrosis,” *Paediatr Respir Rev*, vol. 8, no. 1, pp. 24–29, Mar. 2007, doi: 10.1016/j.prrv.2007.02.009.
- [131] B. K. Rubin, “Mucus structure and properties in cystic fibrosis,” *Paediatr Respir Rev*, vol. 8, no. 1, pp. 4–7, Mar. 2007, doi: 10.1016/j.prrv.2007.02.004.
- [132] H. B. Paz, A. S. Tisdale, Y. Danjo, S. J. Spurr-Michaud, P. Argüeso, and I. K. Gipson, “The role of calcium in mucin packaging within goblet cells,” *Exp Eye Res*, vol. 77, no. 1, pp. 69–75, Jul. 2003, doi: 10.1016/S0014-4835(03)00084-8.

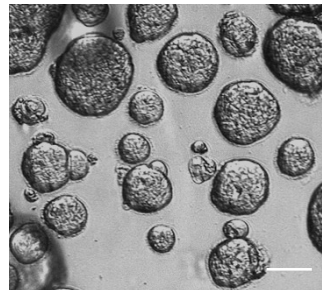
### 5.1 HT-29 MTX spheroids in BSM and alginate

A

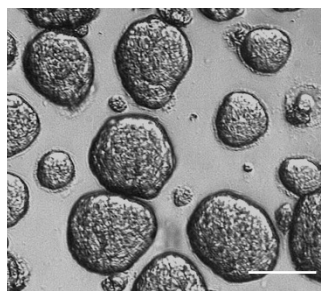
HT-29 in BSM



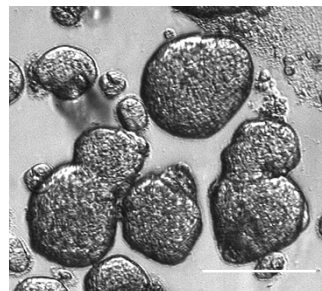
Day 0



Day 3



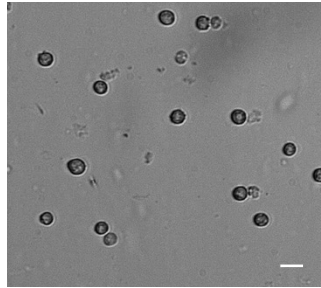
Day 7



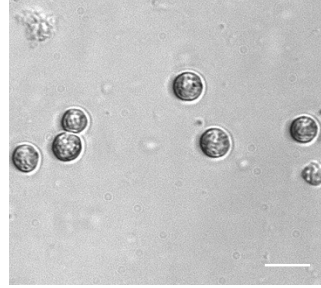
Day 10

B

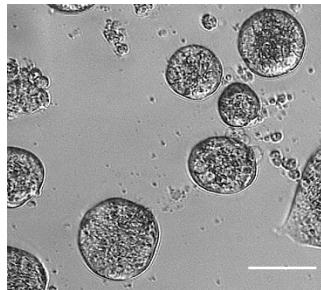
HT-29 in alginate



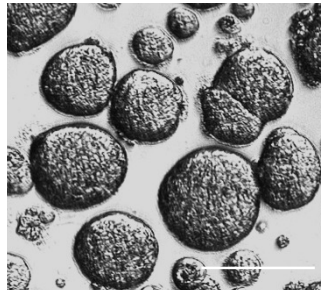
Day 0



Day 3



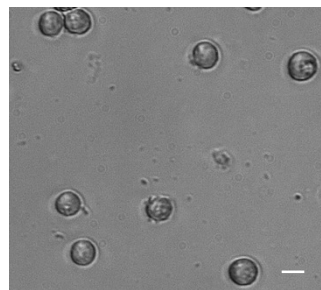
Day 7



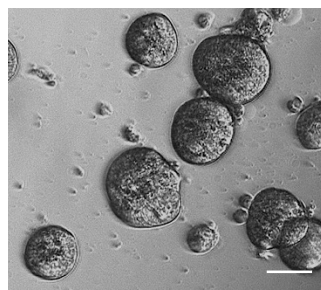
Day 10

C

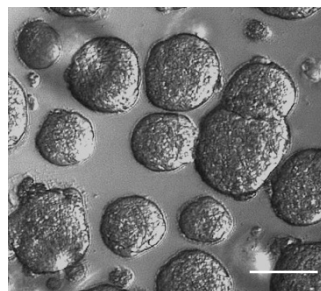
LS174T in BSM



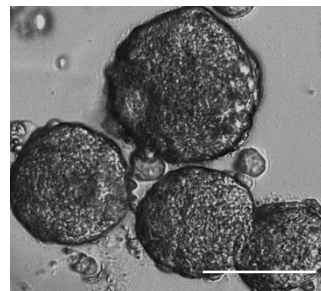
Day 0



Day 3



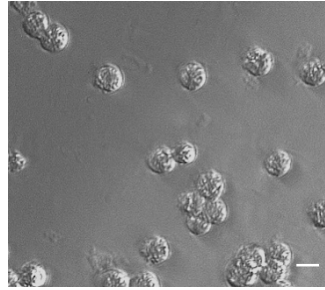
Day 7



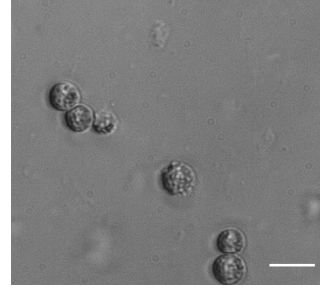
Day 10

D

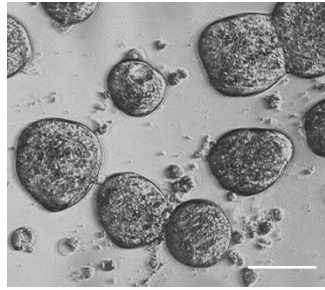
LS174T in alginate



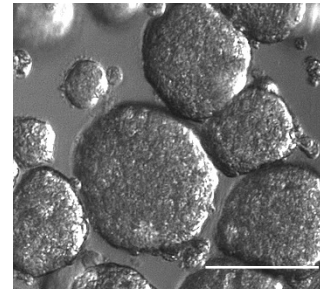
Day 0



Day 3



Day 7



Day 10

Figure 5.1 Images taken under a bright field microscope to observe HT-29 spheroids encapsulated in BSM (A), alginate (B) as well as LS174T spheroids encapsulated in BSM (C) and alginate (D) hydrogels from day 0 to day 10 of encapsulation. Scale bars: 100, 200, 300 and 500  $\mu\text{m}$ , respectively.

## 5.2 Effect of 5-FU in CRC cells

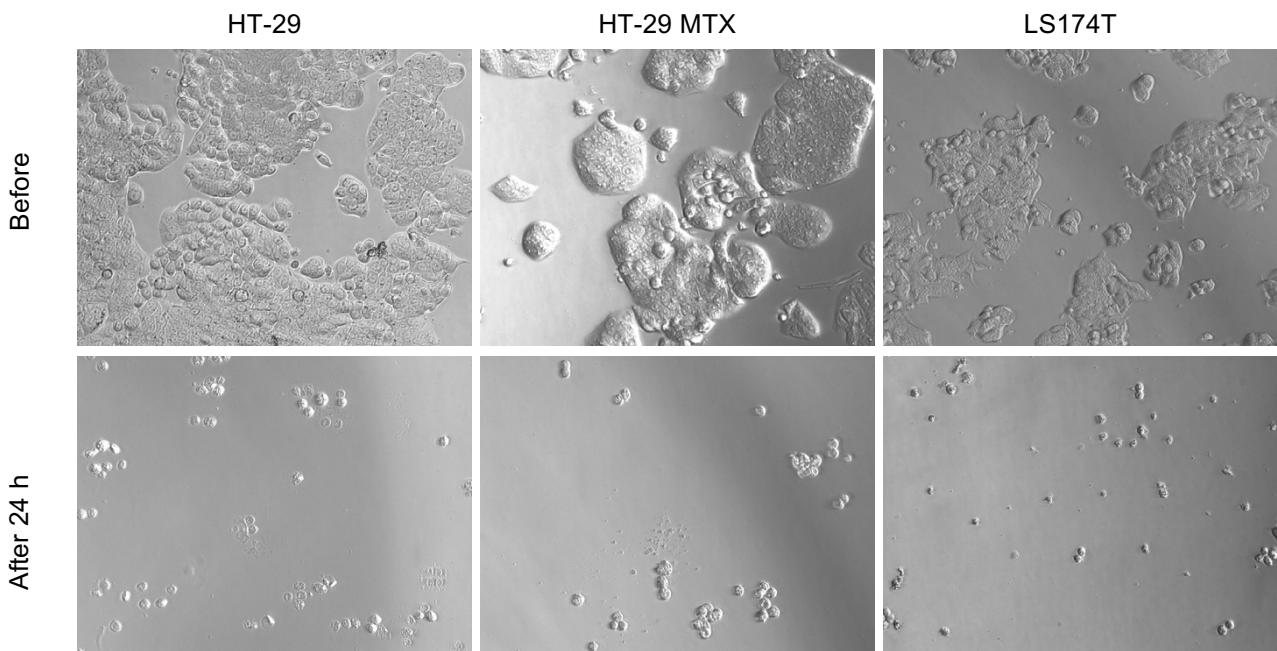


Figure 5.2 The cytotoxic effect of the drug 5-FU in all three CRC cell lines. The first condition shows the cells before the drug treatment. The second condition shows the cells after a 24 h incubation with 50 mM of 5-FU.

### 5.3 Challenge of 2D model with 5-FU

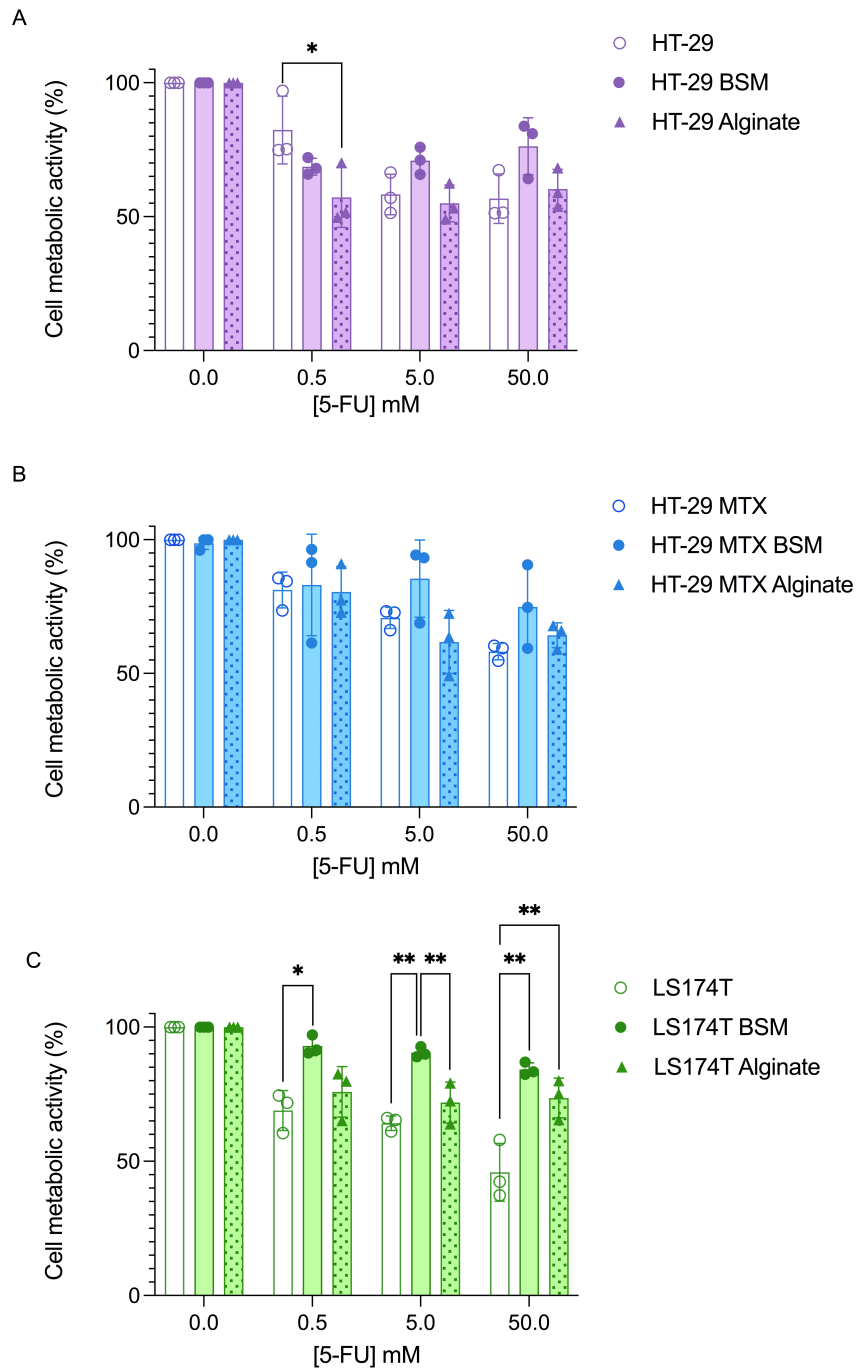


Figure 5.3 Complete drug resistance assay performed on the 2D culture model in three different conditions: absence of gel, presence of BSM or alginate. 5-FU was administered at different conditions: 0.0 mM, 0.5 mM, 5 mM and 50 mM with a normalization to the control (0.0 mM). The error bars designate the standard deviation as obtained from measurements of  $n = 3$  independent experiments. Statistical significance was obtained by one-way ANOVA test by Prism 9.0. \*, \*\*, \*\*\*, and \*\*\*\* indicate  $p$  values of  $<0.0332$ ,  $0.0021$ ,  $0.0002$ , and  $0.0001$ , respectively.

#### 5.4 Staining CRC cells previously exposed to Muc- or Alg- gels with MDR-1

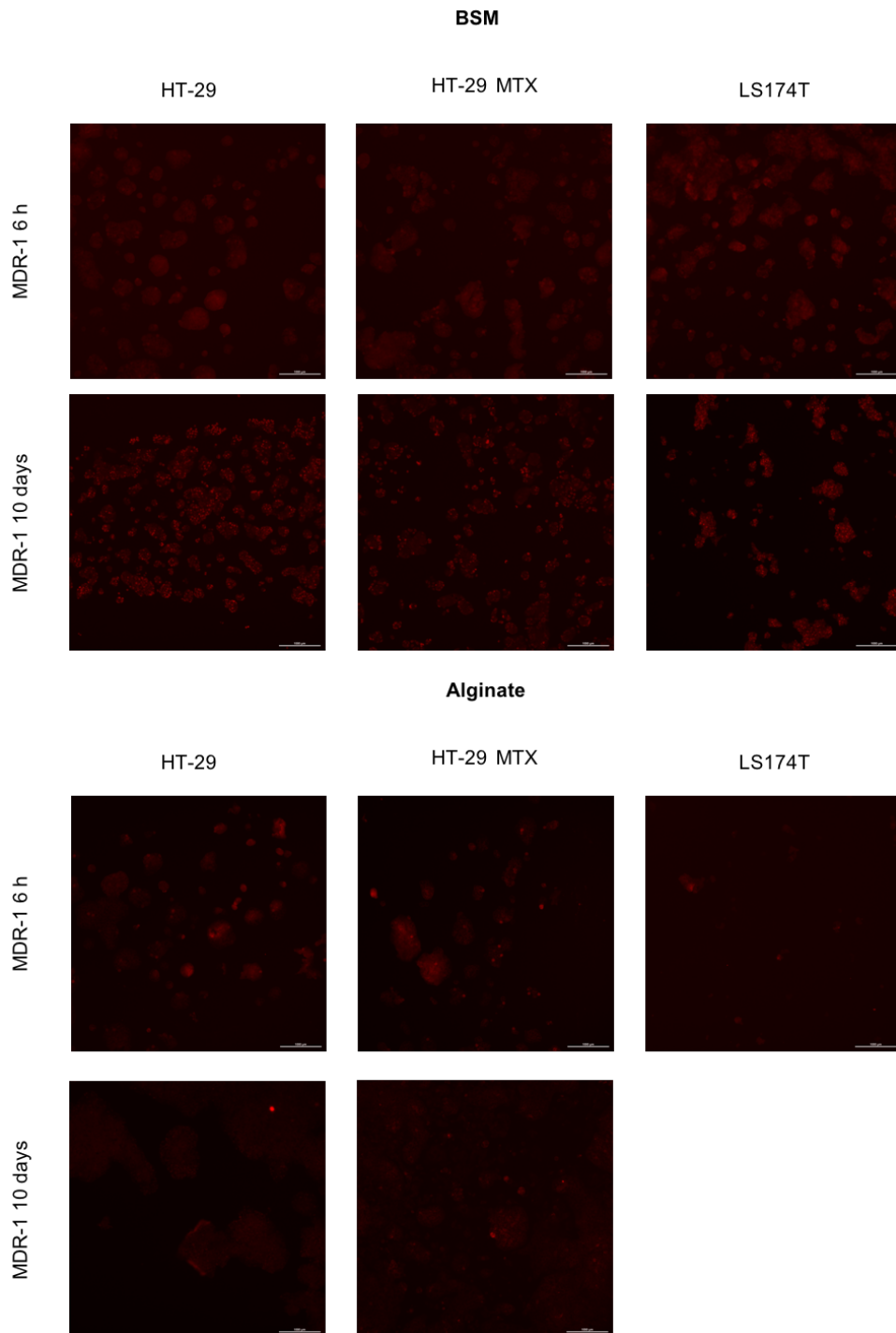


Figure 5.4 Fluorescence microscopy images of MDR-1 expression in HT-29, HT-29 MTX and LS174T cells in BSM and alginate. The cells were covered by each hydrogel for 6 h or 10 days and the immunofluorescence assay was performed following the removal of hydrogel from the monolayer of cells. Scale bar = 1000  $\mu$ m.



## 5.5 Staining CRC cells previously exposed to muc- or alg-gel with CD44

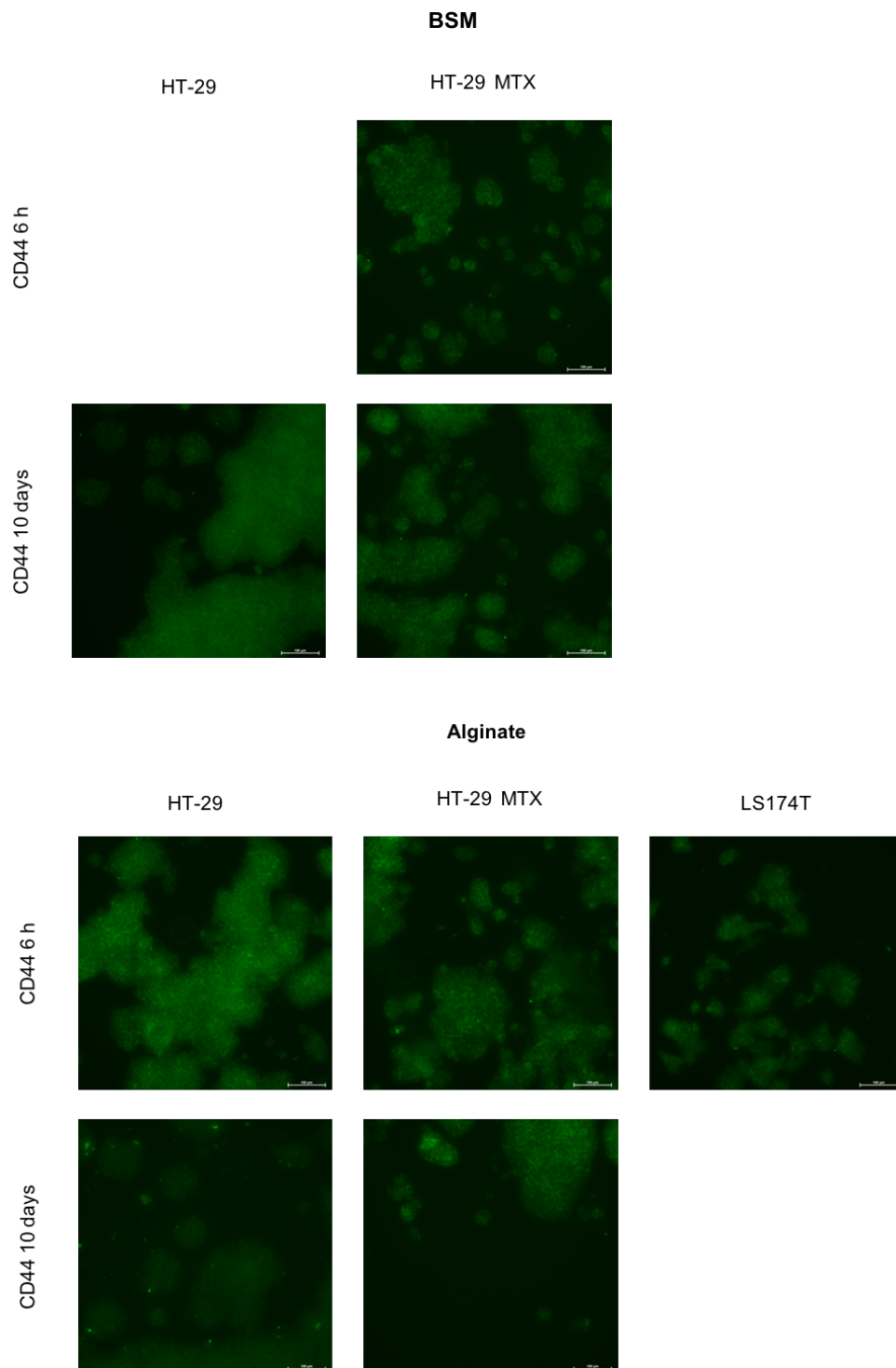


Figure 5.5 Fluorescence microscopy images of CD44 expression in HT-29, HT-29 MTX and LS174T cells in BSM and alginate. The cells were covered by each hydrogel for 6 h or 10 days and the immunofluorescence assay was performed following the removal of hydrogel from the monolayer of cells. Scale bar = 100  $\mu$ m.